A wind-driven perspective on the Atlantic Meridional Overturning

Modelling eddy induced deep layer transport with HIM

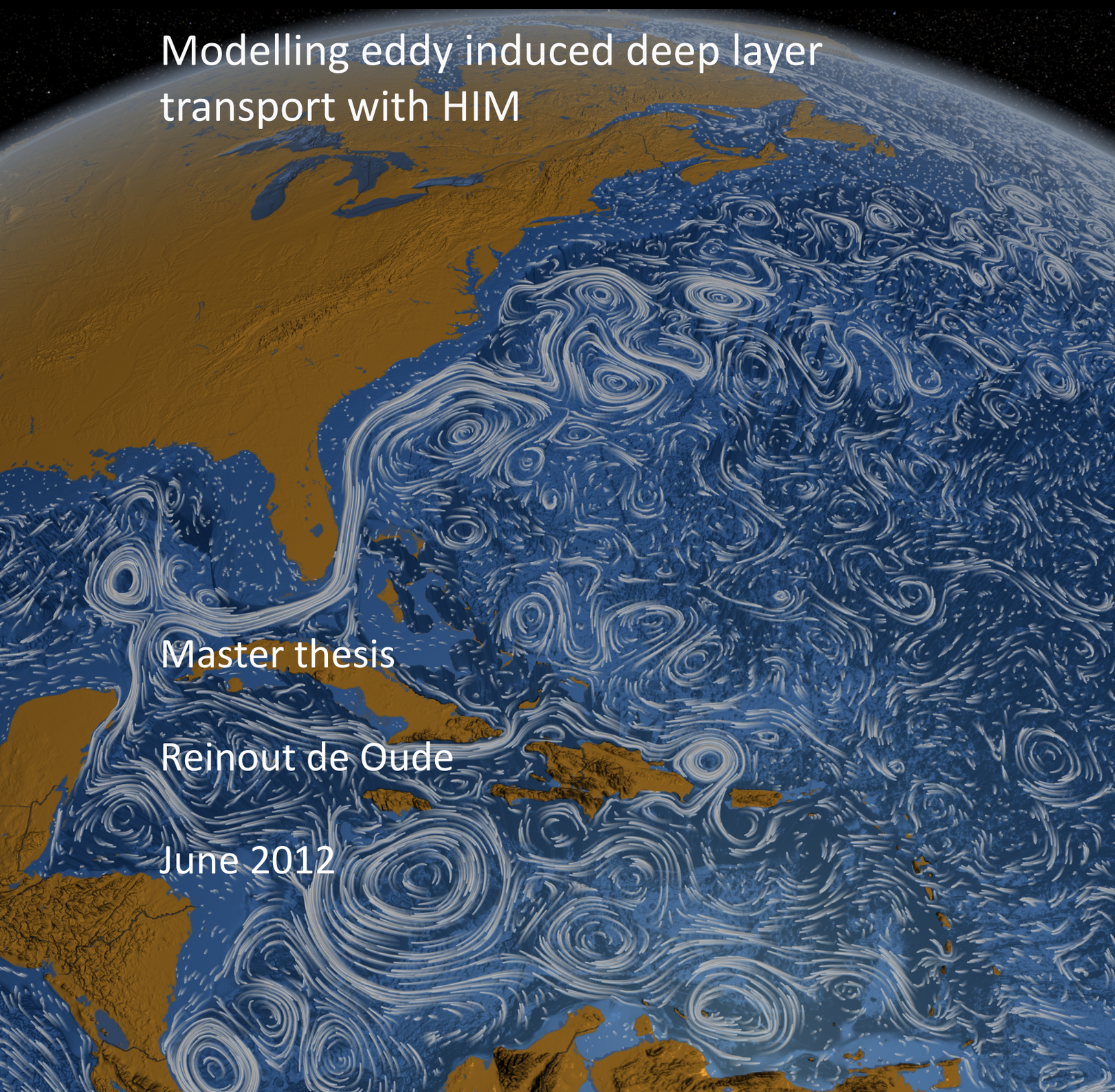

Master thesis

Reinout de Oude

June 2012

A wind-driven perspective on the Atlantic Meridional Overturning

Modelling eddy induced deep layer transport with HIM

Final Report

Den Haag, June 2012

Master thesis of:
R. de Oude MSc

Supervisors:

Prof. Dr. W.P.M. de Ruijter
Oceanic circulation
Institute for Marine and Atmospheric Research Utrecht (IMAU)

D.M. Le Bars MSc
Oceans and Climate
Institute for Marine and Atmospheric Research Utrecht (IMAU)

Universiteit Utrecht

Front cover: NASA 2012

Summary

This study analyses the wind-driven forcing which creates a transport in the deep ocean layer. For long time the thermohaline circulation was considered to be the driving force of the deep ocean. The thermohaline circulation is driven by differences in buoyancy between lower and higher latitudes. The surface gyres create a net northward transport and as a result a net southward deep layer transport in order to close this system. Several studies however have shown that the deep ocean transport shows a circulation that cannot be explained by the buoyancy forcing alone. A numerical study by Holland (1978) showed that eddies play an essential role in deep ocean transport. That study showed that due to the wind forcing eddies develop by baroclinic and barotropic instability. These eddies are able to transfer energy from the surface to the deep ocean and drive a circulation in the deep ocean layer. Other studies and observations confirm the result of Holland (1978) leading to the assumption that eddies induce a deep layer transport.

In this study this deep layer circulation is analysed in order to determine whether this wind driven circulation can acts a mechanism of forcing a circulation resembling the meridional overturning circulation. This study is done by the use of a 2 layer isopycnal model, HIM (Hallberg Isopycnal Model). HIM is based on the primitive Boussinesq equations. The model domain ranges from 60^{o}W to 40^{o}W and 25^{o}N to 55^{o}N in order to mimic the North Atlantic Ocean. The domain has a surface layer of 1000m and a deep layer of 2000m with a density difference between the two layers of 5 kg m^{-3}. The only forcing is a wind forcing with maxima of 0.3 N m^{-2} at 40^{o}N and -0.3 N m^{-2} at 25^{o}N and 55^{o}N in order to create a 2 gyre system with a free eastward jet at 40^{o}N.

The result of this wind forcing provides a gyre structure in the surface layer, an anti-clockwise circulation for the subpolar gyre and clockwise circulation for the subpolar gyre, both gyres with a western intensification. The wind forcing drives the surface layer and creates eddy kinetic energy that drives the deep layer with a gyre structure. This result shows the deep ocean circulation and deep counter current are due to eddy forcing and not due to the MOC.
The deep western boundary currents and recirculation cells provide a southward transport of tracer in the deep layer. The tracer flows via the interior into the subpolar gyre and crosses the jet via the interior. In the subtropical gyre the tracer flows westward in order to flow further southward in the deep western counter current. The tracer is well able to cross the eastward jet; further analysis however showed that the tracer is not able to flow across a westward jet.

In addition to the model analysis a comparison is made with measurements conducted by the RAPID programme over an array at 26.5^{o}N. By the RAPID programme the MOC is calculated by the summation of the Gulf Stream transport, the mid-ocean transport and the Ekman transport. An implementation of the MOC calculation in the model shows that here the Gulf Stream transport is closely in balance with the mid-ocean transport. This shows that the Ekman transport should not be considered as a contribution to the MOC. If the Ekman transport is not considered to be part of the MOC, this reduces the MOC by 3 Sverdrup and decreases its variability. The variability of the measured MOC and modelled volume transport shows similarities in both energy and frequencies, this relation partly increases if the MOC without Ekman transport is analysed.

Overall the wind driven transport in the deep ocean cannot create a MOC-like circulation. The results however do show that several elements of the MOC are in fact forced by eddies in the deep ocean which originate from the wind forcing.

Preface

After extending my student life with an extra master, this master thesis marks the end of a very joyful student life. I enjoyed the extra master in Meteorology, Physical Oceanography and Climate after my first study in Civil Engineering. This master thesis is the result of 8 months studying the transport in the deep ocean. At first, finding a topic was not easy but after a meeting with Will de Ruijter about his ideas concerning the wind driven deep ocean transport, I knew wanted to dive into the deep ocean. The study was very interesting and I learned a lot during this study. I enjoyed modelling the schematized ocean and got a nice experience working with NCL.

By this way I would like to thank my supervisors Will de Ruijter en Dewi Le Bars. Will, thank you for your calm and clear explanations of all the physical aspects I knew about but did not fully understand. Thank you for your enthusiasm about the project and the comments you gave on my results. Dewi thank you for all your help with the model and NCL and for all the useful advice and comments you gave on the project.

Finally I would like to thank my family, girlfriend and friends for their support, enthusiasm and the great times!

Enjoy reading!

Reinout de Oude
Den Haag, June 2012

Table of Contents

List of symbols

A_H	horizontal friction term
A_V	vertical friction term
C	tracer concentration
d	Ekman layer depth
D	diffusion coefficient
f	Coriolis parameter
g	acceleration due to gravity
H	basin depth
k	vertical unit vector
M	Montgomery potential
t	time
u	horizontal velocity vector
u	zonal velocity
v	meridional velocity
u’	zonal velocity fluctuation
v’	meridional velocity fluctuation
w	vertical velocity
x	rectangular zonal position coordinate
y	rectangular meridional position coordinate
z	vertical position coordinate
α	specific volume
β	variation Coriolis parameter with latitude
ζ	shear
θ	latitude
ξ	surface elevation
ρ	density
ϕ	longitude
τ^x	zonal wind stress
τ^y	meridional wind stress

1 Introduction

This study analyses wind induced deep layer transport in a schematised Atlantic Ocean. This first chapter provides the problem analysis and research outline of this study about analysing the wind driven forcing of the ocean circulation. At first, a description of the current research and knowledge about the meridional overturning is given, followed by a discussion leading to the problem analysis. This provides the objective and research questions, which should lead to a more profound understanding of the driving forces in ocean circulation. The methodology describes tools and methods used for this research while the scope describes the limitations in this research. At the end of this chapter the outline describes the content of each chapter in this report.

1.1 Background: A review of the MOC

In the 18th century for the first time a significant colder temperature of the deep-ocean compared to the sea surface temperature was measured. This was the first indication of a temperature gradient between the deep and the subsurface ocean layer and led to the supposition of Count Rumford that ocean waters overturned (Stommel et al., 1981); water from the equator is cooled at higher latitudes due to cold winds, descending to the ocean floor in the polar areas and flowing equatorward over the bottom of the ocean.

The overturning circulation is often called the thermohaline circulation (Figure 1) by the assumption of buoyancy driven forcing due to fluxes and variations of temperature (thermo) and salinity (haline). The driving force is the high latitude cooling, low latitude heating, causing warm and saline (due to evaporation) water. This is transported poleward by wind-driven surface gyres, these gyres results of wind curl forcing. At the polar areas the water is cooled, causing increase of density and a deep vertical mixing resulting in deepwater formation. In the deep ocean this deepwater flows equatorward and eventually reaches the surface by upwelling in order to close the system.

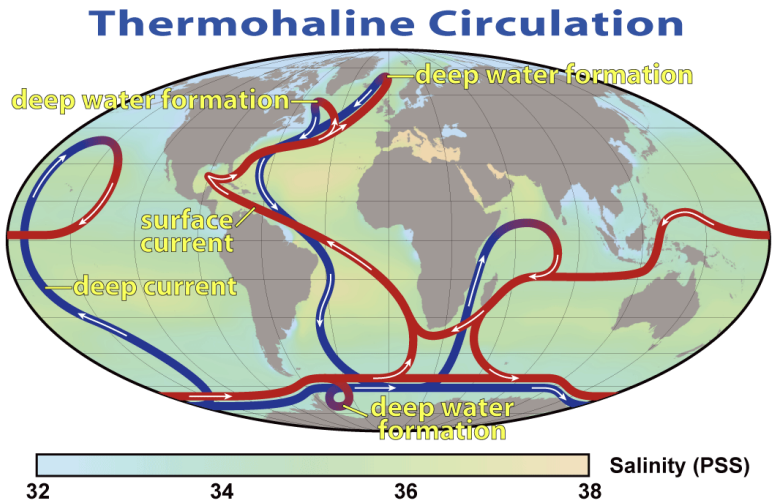

Figure 1 - Pathway of the thermohaline circulation situated along the western boundary, showing the cold deep-water currents in blue and the warm subsurface currents in red.

Since recent time the term meridional overturning circulation (MOC) is used as the two-dimensional flow field with a transport defined as the zonally integrated meridional flux of mass. This term better describes both the wind driven and buoyancy forcing required to acquire this meridional circulation of mass, heat and salinity (Wunsch, 2002).
Since 60 years the lower limb of this overturning circulation seems understood, Henry Stommel showed that ventilated deep waters formed in the polar area are transported equatorward along western-intensified boundary currents (Wunsch, 2002). A study (Broecker, 1987) suggests that the ocean's overturning is important in rapid climate fluctuations, describing the ocean's overturning circulation could flip off due to strong freshwater forcing at higher latitudes. The reduced salinity at higher latitudes would limit the convective mixing and formation of deepwater, breaking down the overturning circulation.

1.2 Problem analysis

For the past several decades, a part of the community embraced the paradigm that the ocean's meridional overturning circulation operates like a conveyer belt, transporting cold water at depth equatorward and warm water from the equator towards higher latitudes, driven by buoyancy changes in the northern latitudes. Several studies have challenged this concept by showing that meso-scale eddies in the ocean, due to the wind-driven gyres in the upper ocean layer, force deepwater currents.

One of the first studies that raised questions about the forcing of the MOC is known as the "Sandström theorem" since 1908 (Wunsch, 2002). This paper provides arguments that, based on the location of heating and cooling of the ocean waters, the solar radiation which penetrates not deeper than 100 meter and the long wave cooling at the surface; the MOC cannot be buoyancy driven. Later on a study (Jeffrey, 1926) found a logical incompleteness, perhaps a flaw in the arguments of Sandstrom and states that physically the MOC could still be buoyancy driven. However an important result of Sandstrom is that he raised the interest in the mechanical forcing (wind and possibly tides) as an important forcing in the abyssal circulation of the ocean and its effect on the MOC.

A numerical study (Holland, 1978) using a wind-driven quasi-geostrophic model provided a general idea about the essential role the eddy fields play in the ocean circulation. The results show how, due to mainly baroclinic instability, eddies develop in the instable region of an eastward jet. These eddies transport energy to the deep ocean and create circulations in the deep ocean.
The results (Holland, 1978) indicate that deep ocean circulations can be due to eddies originating from the wind stress as energy source. This is in agreement with observations (Lozier, 1997), providing the hypothesis that the gyres at intermediate depth of the North Atlantic are an expression of eddy flow. Moreover, the deep circulation is strongly linked to the eddy rich Gulf Stream and North Atlantic Current.

The spatial complexity of the deep ocean circulation is affirmed by (Bower et al., 2009) analysing the pathways of Labrador Sea water (LSW) in the North Atlantic. Measurements by RAFOS floats show that the recently ventilated LSW enters the subtropical gyre via interior pathways instead of via the assumed continuous deep western boundary current. Most floats started in a southward direction according to the deep western boundary current at a depth between 700 and 1500m. However most floats (75%) then escaped the western boundary and followed an

eastward path into the interior along the subpolar-subtropical boundary. Around 24% of the floats reached the subtropical gyre via the interior. This is the largest southward float displacement over two years of study, indicating that the interior is the dominant pathway for LSW to enter the subtropical gyre instead of the long believed deep western boundary current. The floats circulate before entering the subtropical gyre or do not reach this southern gyre at all.

Similar to the results in the North Atlantic, (Biastoch et al., 2008) show that the deep Agulhas undercurrent is not continuous. In this study model results and experiments with numerical floats are carried out results show that there is no continuous deep boundary current, but instead floats seem to follow a (re)circulating structure.

All these studies indicate that the ocean overturning is not solely due to density and temperature gradients. Instead this raises the hypothesis that the deep ocean circulation is driven by eddies due to wind-driven surface gyres. Meridional transport can take place as the deep ocean gyres are connected, creating a pathway for the deep circulation, a pathway which is not confined to the deep western boundary.
These deep layer circulations can transport water from high latitudes in southward direction in the Atlantic, as the surface gyres do in the upper ocean. This way meridional transport exists due to wind driven forcing at the surface, instead of the buoyancy forcing as assumed by the theory of the thermohaline circulation or meridional overturning circulation.

1.3 Objective and research questions

Based on the problem analysis the objective of this study is stated as follows:
Determine by modelling to what degree the wind driven circulation can explain the vertical structure of the circulation across the Atlantic.

In order to achieve this objective three research questions have to be answered:

- To what degree does the wind forcing provide a gyre structure created by eddies in the deep layer?
- To what extend provides the deep layer a meridional transport of a (NADW-like) tracer?
- Can the wind forcing provide a MOC-like circulation and/or can MOC-aspects/variability be explained by the wind forcing?

1.4 Methodology and Scope

In order to conduct this study a multi-layer isopycnal model is used, the so-called Hallberg Isopycnal model (HIM). This model is isopycnal based instead of depth or pressure. The model contains all oceanic processes that influence the large-scale oceanic motion. In order to analyse the effect of wind driven deep ocean circulation only the wind forcing will be the external force in the model. The domain of the model will be a rectangular grid with 2 layers, the orientation is based on North Atlantic but will be of smaller scale and without the contour of any continental land boundaries or topography as both aspects will reduce the computational time. In two experiments the model domain is expanded to a 4 gyre system and a 4 gyre system with continental land boundaries. This is done for tracer analysis in the deep layer and further explained in chapter 7. The domain is based on the North Atlantic in order to make a comparison possible with data obtained over an array in the Atlantic Ocean at 26.5^{o}N. This data is obtained via various ways of measuring which is explained in chapter 6.

1.5 Outline

This study is about analysing the effect of wind-forced eddies in the deep ocean and how eddies drive the deep ocean circulation. In chapter 2 the theoretical basis of this concept (Holland, 1978) is further explain. Chapter 3 describes HIM as well as the model setup for this study, describing the domain, the wind input and all relevant parameters in the model.
Chapter 4 provides the first results and answers to the first research question describing to what extent eddies, created by the wind, provide a gyre structure in the deep ocean layer. Afterwards in chapter 5 the tracer analysis is provided, answering the second research question. In chapter 6 the model results are compared by measured data and the model results are further analysed in order to provide an answer to the third research question, whether the wind forcing can provide a MOC-like circulation and which features of the MOC can be found in the model results. This study ends with the conclusion in chapter 7 with the discussion and recommendations for further research.

2 Theoretical description

In this chapter a theoretical analysis is provided describing how wind forcing on the ocean surface can drive the deep ocean layer. At first the surface forcing and Ekman-transport is described followed with an analysis of the energy in the ocean, resulting into the driving forcing in the deep ocean. Before this analysis is given first the shallow water approximation of the Navier-Stokes equations are given which form a basis for the explanation of the theoretical description.

$$\frac{Du}{dt} - v(f_0 + \beta_0 y) + \frac{1}{\rho_0}\frac{\partial p}{\partial x} = A_H\left[\frac{\partial^2 u}{\partial x^2} + \frac{\partial^2 u}{\partial y^2}\right] + A_V\frac{\partial^2 u}{\partial z^2} \quad (1)$$

$$\frac{Dv}{dt} + u(f_0 + \beta_0 y) + \frac{1}{\rho_0}\frac{\partial p}{\partial y} = A_H\left[\frac{\partial^2 v}{\partial x^2} + \frac{\partial^2 v}{\partial y^2}\right] + A_V\frac{\partial^2 v}{\partial z^2} \quad (2)$$

$$\frac{\partial p}{\partial z} = -\rho g \quad (3)$$

$$\frac{\partial u}{\partial x} + \frac{\partial v}{\partial y} + \frac{\partial w}{\partial z} = 0 \quad (4)$$

Here u and v are the zonal and meridional velocity, w is the vertical velocity, f_0 is the Coriolis parameter, β_0 is the variation of Coriolis parameter with latitude. X, y and z rectangular position coordinates in the east-west, north-south and vertical directions. ρ_0 is density, t is time, g is acceleration due to gravity and A_H and A_v are horizontal and vertical friction terms.

2.1 The surface Ekman layer

Consider an ocean region with interior flow field $(\bar{u}, \bar{v})$ is subject to a wind stress (τ^x, τ^y) along its surface. Assuming steady conditions, a homogeneous fluid and a geostrophic interior, the following equations and boundary conditions for the flow field (u, v) in the surface Ekman layer:

$$-f(v - \bar{v}) = A_V\frac{\partial^2 u}{\partial z^2} \quad (5)$$

$$+f(u - \bar{u}) = A_V\frac{\partial^2 v}{\partial z^2} \quad (6)$$

Surface (z = 0): $\rho_0 A_V\frac{\partial u}{\partial z} = \tau^x, \quad \rho_0 A_V\frac{\partial v}{\partial z} = \tau^y$ (7)

Towards interior ($z \to -\infty$): $u = \bar{u}, v = \bar{v}$ (8)

The solutions of the velocities in the surface Ekman layer (d) are:

$$u = \bar{u} + \frac{\sqrt{2}}{\rho_0 f d}e^{z/d}\left[\tau^x\cos\left(\frac{z}{d} - \frac{\pi}{4}\right) - \tau^y\sin\left(\frac{z}{d} - \frac{\pi}{4}\right)\right] \quad (9)$$

$$v = \bar{v} + \frac{\sqrt{2}}{\rho_0 f d}e^{z/d}\left[\tau^x\cos\left(\frac{z}{d} - \frac{\pi}{4}\right) + \tau^y\sin\left(\frac{z}{d} - \frac{\pi}{4}\right)\right] \quad (10)$$

The velocities in the surface Ekman layer are proportional to the Ekman layer depth d, and may be very large. The wind-driven horizontal transport in the surface Ekman layer has components given by:

$$U = \int_{-\infty}^{0}(u - \bar{u})\,dz = \frac{1}{\rho_0 f}\tau^y \quad (11)$$

$$V = \int_{-\infty}^{0} (v - \bar{v})\, dz = -\frac{1}{\rho_0 f}\tau^x \tag{12}$$

This shows that the transport is orientated perpendicular to the wind stress, to the right in the Northern Hemisphere and to the left in the Southern Hemisphere.
The divergence of the flow is determined by integrating over the Ekman layer:

$$-w_{Ek} = \int_{-\infty}^{0} \left(\frac{\partial u}{\partial x} + \frac{\partial v}{\partial y}\right) dz = \frac{1}{\rho_0}\left[\frac{\partial}{\partial x}\left(\frac{\tau^y}{f}\right) - \frac{\partial}{\partial y}\left(\frac{\tau^x}{f}\right)\right] \tag{13}$$

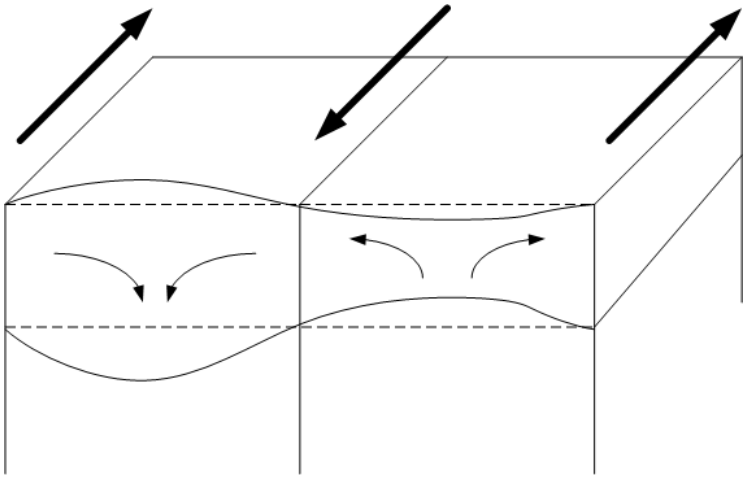

Figure 2 - Downwelling (left) and upwelling (right) due to Ekman pumping as a result of sheared winds.

The divergence is entirely due to the wind stress since the interior geostrophic flow is non-divergent. If the wind stress has a non-zero curl, a vertical velocity results throughout the interior, called Ekman pumping. In the Northern Hemisphere, a wind curl with a negative curl (clockwise pattern) generates convergence which induces downwelling and an increased surface elevation; where as a positive curl (counter clockwise wind pattern) generates divergence which induces upwelling and a decreased surface elevation (see Figure 2).

2.2 Sverdrup balance

The surface elevation creates a pressure gradient which causes a flow according to the thermal wind balance. The equations for zonal en meridional shear by thermal wind balance read as follows:

$$\frac{\partial v}{\partial z} = -\frac{g}{f_0 \rho_0}\frac{\partial \rho}{\partial x} \tag{14}$$

$$\frac{\partial u}{\partial z} = \frac{g}{f_0 \rho_0}\frac{\partial \rho}{\partial y} \tag{15}$$

Due to the increased surface elevation there is a clockwise circulation: the subtropical gyre, around the decreased surface elevation there is an anticlockwise circulation: the subpolar gyre. The system resulting into these gyres is called the Sverdrup flow.

$$\beta_0 v = \frac{1}{\rho D}\left(\frac{\partial \tau^y}{\partial x} - \frac{\partial \tau^x}{\partial y}\right) \tag{16}$$

This gyre setup is now close to what is observed in the ocean except one crucial element, the land boundaries and the resulting western intensification.
The western intensification is the result over the varying Coriolis parameter with latitude, $\partial f / \partial \phi$ or β. This can be best explained by the use of vorticity, i.e. spin, in the subtropical gyre (Figure 3).

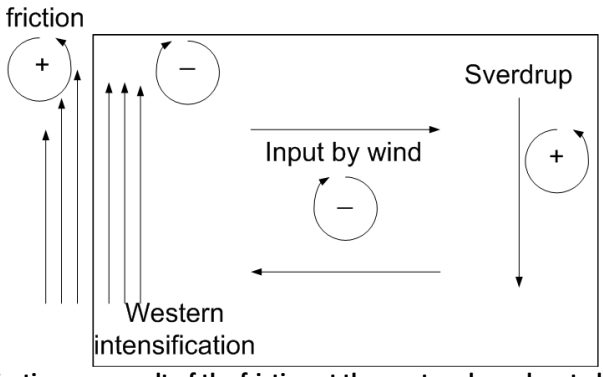

Figure 3 - Western intensification as a result of the friction at the western boundary to balance the vorticity induced by the wind.

The wind stress induces a clockwise rotation or negative vorticity. This vorticity has to be taken out by an opposite vorticity created by friction. This vorticity can be created by strong friction along the western boundary and for strong friction to occur a strong current along the western boundary is required; the western intensification. This strong northward current itself has a negative vorticity, which is compensated by the southward Sverdrup flow in the interior. An eastern intensification would not be possible as friction on the eastern boundary would create negative vorticity which cannot balance the negative vorticity of the wind stress. Stommel was in 1948 the first to present this adequate explanation for this feature (Pond, 1978).

2.3 Baroclinic and Barotropic instability

The western boundary intensification creates an eastward jet in-between the subpolar and subtropical gyre. This jet creates a first mechanism of instability, barotropic instability. This barotropic instability is created by a horizontal shear, as with a jet the zonal velocity varies over the latitude. The shear creates vorticity and if this vorticity overcomes the vorticity induced by the β-parameter (planetary vorticity) barotropic instability can occur. Due to this instability eddies are generated by shear in the mean flow and gain their energy from the mean flow kinetic energy.
A second mechanism of instability is the baroclinic instability; this is created by the vertical shear. This type of instability can occur in a stratified flow with distinct density layers; in this study a two layer model is used. Due to the vertical shear there is a velocity difference between two layers. The resulting thermal wind balance creates a gradient in the interface between the two layers. This gradient of interface allows eddies to grow which draw its energy from the mean potential energy.
The two types of instability can both occur and will balance each other. Therefore both will contribute to the development of eddies which transport energy to the deep layer. The effect of the barotropic instability is to broaden, and weaken the jet. For the baroclinic instability, the energy source is the potential energy of the basic state, this instability would generally sharpen the jet profile. The two mechanisms can be thought of as providing a balancing scheme. A jet which is very broad but with vertical shear will become unstable and reduce the vertical shear but sharpen the jet. A sharp jet becomes barotropically unstable producing a broader jet.

2.4 Energy partition in the ocean

In order to drive the deep layer of the ocean, an energy source is required. The basis in this study is that only wind forcing on the surface can deliver this required energy. As is described the wind gives an input of energy creating the Sverdrup flow and the Ekman transport.

Some first results of Holland (1978) show that there is hardly any transfer of kinetic energy from the surface to the deep layer (K_1 -> K_2 = 0, Figure 4). However most of the kinetic energy is converted to potential energy, which is in accordance with (Gill et al., 1974). The baroclinic instability creates eddy activity near the interface and these eddies draw energy from the available potential energy and turn this into eddy kinetic energy in the deep layer. As a result the deep ocean eddy kinetic energy is created.

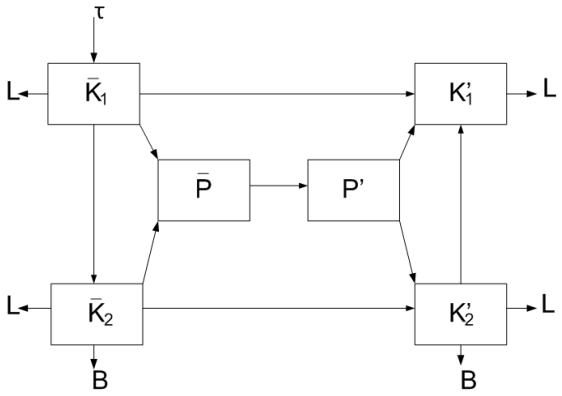

Figure 4 - Energy partition describing the kinetic energy in the surface (1) and deep (2) layer and the potential energy.

The interpretation of this result can be explained by the changing thermocline in Figure 2. The average potential energy is proportional to the mean square displacement of the interface whereas the average kinetic energy is proportional to the mean square slope of the interface.
In the eastward jet eddies are expected due to the baroclinic instability. These eddies will create a large amount of eddy kinetic energy as these are of small length scale with a steep slope in the interface. The kinetic energy is transferred downward providing energy to the currents and circulations in the deep ocean (Holland, 1978). As described there can be direct transport of kinetic energy by eddy kinetic energy to the deep layer due to the barotropic instability. However the result of (Holland, 1978) show that the baroclinic instability is the dominant term of instability.

3 HIM Model

This chapter provides a brief description of the model HIM, describing its basis equations and computation grid. In addition the model setup is given, providing a description of the model domain and the wind forcing.

3.1 Model description

The Hallberg Isopycnal Model (HIM) is a programme that simulates the ocean by numerically solving the Boussinesq equations in isopycnal vertical coordinates and general orthogonal horizontal coordinates. The isopycnal model makes use of the potential density referenced to a given pressure as the vertical coordinate. This system basically divides the water column into distinct homogeneous layers, whose thicknesses can vary from place to place and from one time step to the next.

These basic equations behind this model are the inviscid, unforced primitive Boussinesq equations in isopycnal layers, these are based on the Navier-Stokes equations. The Boussinesq equations read as follows:

$$\frac{\partial \boldsymbol{u_n}}{\partial t} + \boldsymbol{u_n} \cdot \nabla \boldsymbol{u_n} + f\hat{\boldsymbol{k}} \times \boldsymbol{u_n} = -\nabla \boldsymbol{M_n} \tag{17}$$

$$\frac{M_{n+1} - M_n}{\alpha_{n+1} - \alpha_n} = p_{n+1/2} \tag{18}$$

$$\frac{\partial}{\partial t}(\Delta p_n) + \nabla \cdot (\boldsymbol{u_n} \Delta p_n) = 0 \tag{19}$$

Where $\boldsymbol{u}$ is the horizontal velocity in vector notation, f is the Coriolis parameter, $\hat{\boldsymbol{k}}$ is a vertical unit vector, p is pressure, α is the specific volume (inverse of density) and $M \equiv \alpha p + gz$ is the Montgomery potential. The subscripts indicate the layer with an index that increases downward. A half-integer subscript indicates the value at the interface. The specific volume, α, is a constant within each layer, but $\boldsymbol{u}$, M and p vary in the horizontal (Hallberg, 1997). The described equations (17 -19) are the basis to calculated the energy in the model for each layer and the required eddy kinetic energy in the deep layer.

The model makes use of general orthogonal horizontal coordinates where θ is latitude and ϕ is longitude. The equations are horizontally discretized on an Arakawa C-grid. In this grid the meridional velocity v is evaluated at the centres of the upper and lower grid faces, the zonal velocity u is evaluated at the centres of the left and right grid faces. The relative and potential vorticity is evaluated at the grid points and the height of the interfaces at the centre of the grid cells.

3.2 Model setup

The model domain is defined by a grid with a resolution of 1/5° and stretches from 60°W to 40°W in longitude and from 25°N to 55°N in latitude. For two experiments in this study this domain is changed, this will be described for each experiment later on. The ocean is schematised by two layers; one surface layer of 1000 meter deep and deep layer of 2000 meter making a total ocean depth of 3000 meter (see Figure 5). The two layers are characterised by different densities, the surface layer has a density of 1030 kg m^{-3} and the deep layer a density of 1035 kg m^{-3}. By this schematisation the interface between the layers mimics the thermocline.

The shape of the wind forcing is also provided in Figure 5. The wind forcing has a sinusoidal distribution over the domain and has maximum at 40°N in the eastward direction and two maxima in the westward direction at 25°N and 55°N. This way a 2 gyre system will be created with a eastward jet at 40°N. The maximum wind forcing can vary for different experiments but the sinusoidal shape will remain intact. In appendix A a list of parameters and constants are given which are used in the model.

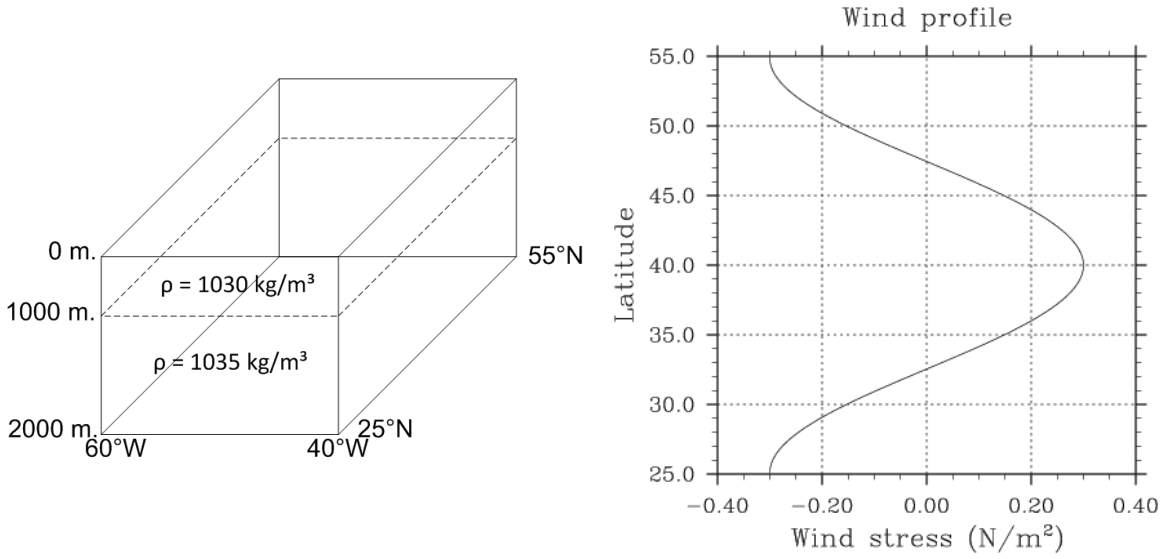

Figure 5 – Schematization of model domain and wind forcing over the domain

4 Circulation in the deep layer

In this chapter the first research question will be analysed; to what degree will wind driven eddies create a gyre structure in the deep layer. This is investigated with use of the HIM model as described in chapter 3. In this chapter first the setup of the model will be analysed, resulting in an overview of the flow velocity and the eddy kinetic energy followed by the analysis of the meridional volume transport in both the surface and deep layer.

4.1 Results of wind forcing

The first step of modelling is to obtain the appropriate wind forcing in order to achieve realistic flow velocities in the top layer of the ocean. A realistic maximum flow velocity considered to take place in the western boundary current is assumed to be a flow velocity of 1 ms^{-1}. Three different wind forcing of τ = 0.1, 0.2 and 0.3 Nm^{-2} are used to analyse the corresponding velocities.

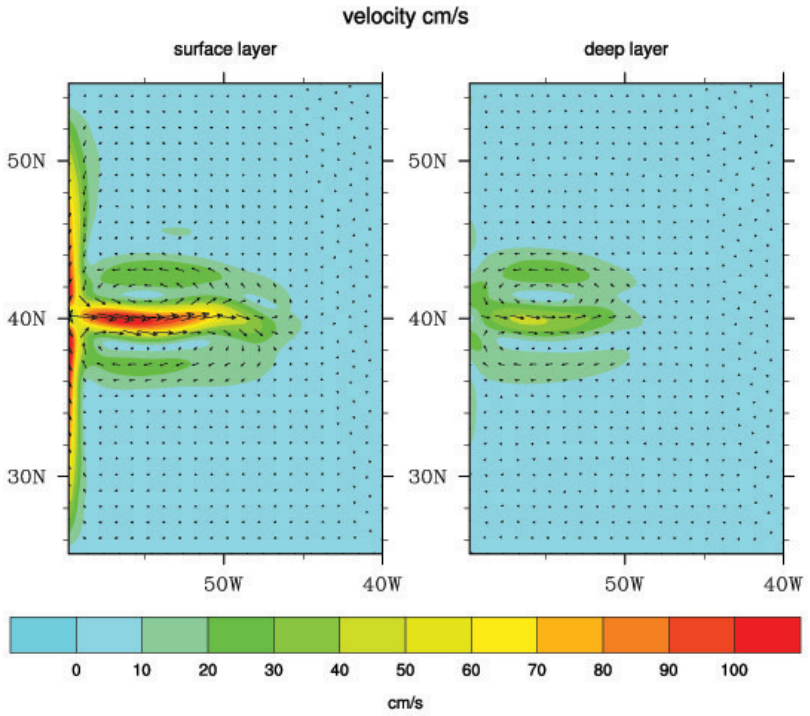

Figure 6 - velocity map for τ = 0.3 N m^{-2} for surface (left) and deep layer (right).

Figure 6 shows the flow velocity of the surface and deep layer by a wind forcing of 0.3 Nm^{-2}. This wind forcing produces the assumed flow velocities of 1 ms^{-1} in the western boundary current, which is comparable to the Gulf Stream. The wind forcing of 0.1 and 0.2 N m^{-2} resulted in significant lower flow velocities of respectively 0.5 and 0.7 ms^{-1} (see Appendix B). Figure 6 shows a strong western boundary current in the surface layer for both the subpolar and subtropical gyre, these two currents converge into a free eastward jet at 40°N. This jet extends eastward to around 48°W where a quite strong recirculation start; clockwise in the subtropical gyre and counterclockwise in the subpolar gyre. The interior shows the compensating circulation (the Sverdrup flow) which has a lower velocity than the recirculation.

Figure 6 shows a flow in the deep layer, similar to the surface layer with an eastward jet at 40N and the recirculation. This shows that the eddy kinetic energy is transported downward and

drives a deep layer circulation. As expected the flow velocities in the deep layer are smaller than to those in the surface layer.

4.2 Eddy kinetic energy

Figure 7 shows the eddy kinetic energy in both the surface (left) and deep (right) layer. The eddy kinetic energy (EKE) is a measure for turbulence and is defined as:

$$EKE = \sqrt{\frac{u'^2 + v'^2}{2}} \tag{20}$$

In which u'and v' are the zonal and meridional velocity fluctuation related to the time averaged mean velocities.

The results confirms the assumption in chapter 2 that the wind forcing and baroclinic instability are able to generate eddy kinetic energy in the surface layer which are transported in to the deep layer, causing a horizontal flow in the deep layer. The eddy kinetic energy is mainly at the location of the jet as here the largest baroclinic instability takes place. The contour lines in the figure indicating the change in surface and interface height compared to the initial situation, these lines confirm the downwelling in the subtropical gyre and the upwelling in the subpolar. These results are quite a good reproduction of similar results (Holland, 1978) in a quasi-geostrophic model showing very similar patterns for the steady state as those presented in Figure 7.

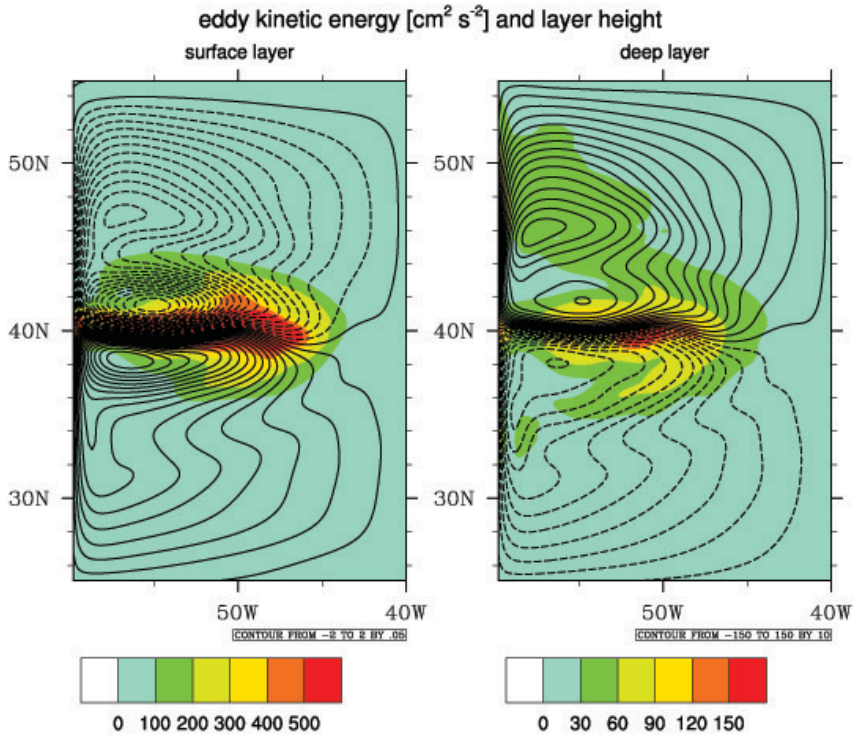

Figure 7 - Eddy kinetic energy and the contour lines of the change in surface height ranging from -2 to 2 meter by 0.05m inervals (left) and change of interface depth ranging from -100 to 100 meter by 10m intervals (right).

The strong gradient of the interface is confirmed in Figure 8 which gives the height of the interface over the latitude at 55°W. At this longitude the interface displacement is largest as is visible in Figure 7. The graph shows a very steep slope over 39°N to 41°N, here the displacement changes from a depth of 1100 meter to a depth of 850 meter. Outside of this region the slope is rather mild. The strong gradient, as described in chapter 2, is the required condition to draw a lot of eddy kinetic energy from the available potential energy as shown in Figure 7.

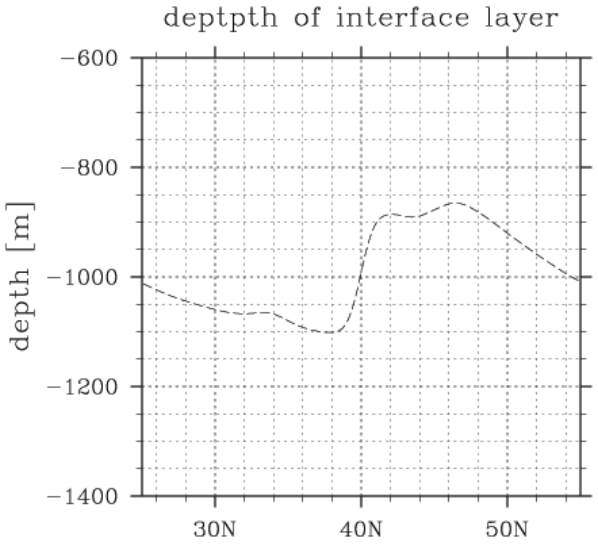

Figure 8 - depth of interface layer, showing downwelling in the subtropical gyre and upwelling in the subpolar gyre.

4.3 Volume transport in 2 gyres system

With the eddy kinetic energy driving the deep ocean layer and the resulting velocity field it is of interest to analyse the resulting meridional volume transport in the deep layer. The volume transport is defined as the time-averaged (1 month) velocity multiplied by the depth of the layer and grid width ($1/5^0$) resulting in a volume transport in Sverdrup (Sv). The meridional volume transport describes the northward (positive) and southward (negative) flow of water. The result of a 5 years average is presented in Figure 9.

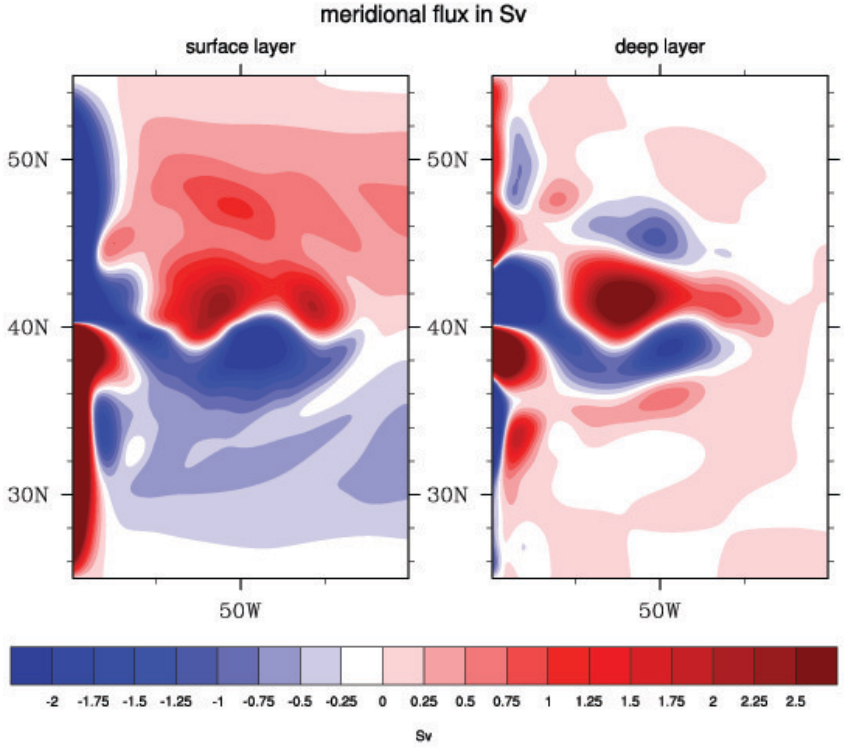

Figure 9 - Meridional volme transport in Sverdrup for the surface (left) and deep layer (right).

The results for the surface layer are well understood, the map clearly show the two western boundary currents resulting in a free eastward jet at 40°N and a weaker counter current in the interior. At the location 40°N°, 50°W the map shows the recirculation currents with a strong northward (subpolar gyre) and southward (subtropical gyre) flow. In the interior the western boundary currents are balanced by the Sverdrup flow

The map of the deep layer shows that the meridional volume transport has a different pattern than the surface layer. Near the location of the eastward jet (37°-43°N) two recirculation cells develop; in the subpolar gyre the recirculation cell has a counterclockwise motion, with a strong northward flow in the interior and a southward western boundary current (43°N-40°N). In the subtropical gyre the recirculation has a clockwise circulation with a southward flow in the interior and a northward western boundary current (37°-40°N). Further south and north of these recirculation cells secondary recirculation cells develop with a counter circulation compared to the first recirculation cell. These secondary recirculation cells create a northward deep counter current north of 43°N and a southward deep counter current south of 37°N.

This result show that deep western boundary currents are wind driven, induced by eddies, including deep counter currents. This also explains why the deep boundary current is not a continuous flow from north to south, but instead varies from direction over the latitudes.

The time-averaged results of the meridional volume transport show a connecting cross-gyre southward transport over the eastward jet in both the surface and deep layer. This indicates the possibility of southward transport of tracer in the deep layer. In the following chapter the tracer transport is further analysed.
Overall, in the surface layer there is a gyre structure that consists of a Sverdrup flow and recirculation near the jet. In the deep layer there are recirculation cells due to the eastward jet which is created by eddy kinetic energy.

5 Tracer transport in the deep layer

In this chapter the pathways of a tracer is analysed. The objective is to mimic the transport of North Atlantic Deep Water, which is considered as an indication of the overturning in the North Atlantic and which can be followed up to the South Atlantic Ocean. To compute the transport a passive Eulerian tracer is added to the model. The tracer transport is based on the basic advection-diffusion equation:

$$\frac{\partial C}{\partial t} = D\nabla^2 C - \boldsymbol{u}\nabla \mathrm{C} \tag{21}$$

here c is the concentration of the tracer and D is the diffusion coefficient. In this study the advection is the dominant element of the tracer transport. In the model a tracer is added in the northern region of both layers; in the region between 53° and 55°N over the whole width of the domain the value of tracer is fixed to 0. South of 32°N the tracer is removed by fixing its value to 0. In this chapter the concentration and pathway of the tracer is analysed.

5.1 Tracer transport in 2 gyres system

In this experiment the tracer is added to the model results of the 2 gyre system as analysed in Chapter 4. The tracer is characterised by a value of 1, while the normal water is characterised by a value 0. In the southern region of the domain the tracer is removed by defining the area south of 32N always with value 0. This way the domain does not fill up with tracer and the deep pathways of tracer can be well analysed.

The model run shows that the required time for the tracer to achieve a statistical equilibrium is 25 years. After these years a 5 years average of the meridional tracer transport, defined as the volume transport multiplied with the value of tracer (units in Sverdrup), is taken and presented in Figure 10.

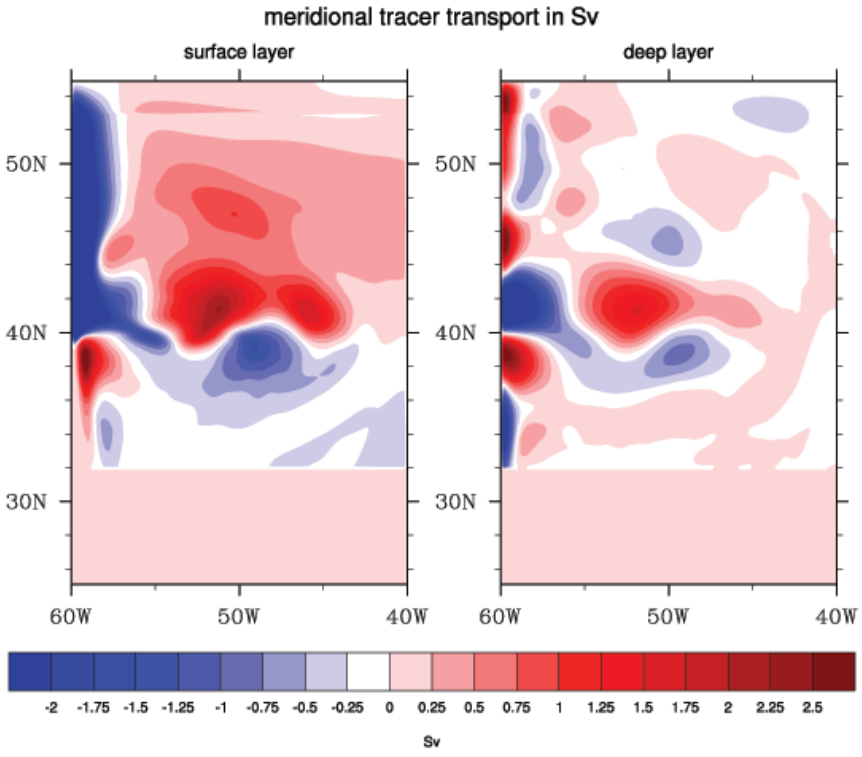

Figure 10 - Meridional tracer transport for the surface (left) and deep layer (right).

The maps of tracer transport for both layers show similar patterns as in Figure 9. However these results show the actual pathways of tracer transport, showing e.g. that a southward flux in the subtropical gyre originates from the subpolar area of 53°-55°N and thus proofs that the recirculation cells are connected. In the surface layer the results show a southward transport of tracer in the western boundary current which is able to cross the eastward jet, and propagate further southward in the interior of the subtropical gyre.
The map of the deep layer shows that tracer is transported southward via the southward branches of the secondary recirculation cells. This is via the interior at 52°W and close to the western boundary at around 58°W. Via these two branches of the secondary recirculation cells the tracer is transported toward the jet where it experience the first recirculation cell, here most of the tracer is transport around the jet and flows via the eastern side of the jet in the subtropical gyre. Once east of the jet, the first recirculation cell in the subtropical gyre picks up the tracer transporting it to the western boundary where it flows southward via the deep counter current, from 36°N and southward.

This result is agreement with the observations (Bower et al., 2009) as described in Chapter 1. In that study, floats released in the Labrador Sea reached the subtropical gyre via the interior instead of the deep western boundary current as first was assumed. The floats were released in the northwest region of the Atlantic Ocean and flowed southward via the deep western boundary current until 43°N. There most of the floats (80%) left this current and flowed into the interior. Via the interior 23% of the floats reached the subtropical gyre, while only 8% of the floats reached the subtropical gyre by the deep western boundary. A similar result is presented here, however the southward flow in the northern region (55°N-47°N) is not in the direct western boundary current but just east of this. However it is under the surface layer boundary current and might therefore be interpreted as the deep western boundary current by (Bower et al., 2009). The bathymetry also influences the location of these currents. Nevertheless the general understanding is similar in the model and observations showing a dominant deep southward flow in the interior instead of the deep western boundary current.
Figure 11 shows the zonal integration of the tracer transport. It shows a rather consistent flow of around 21 Sv in southern direction in the surface layer. In the deep layer the tracer transport is slight decreasing while proceeding southward with an average transport of around 2.5 Sv.

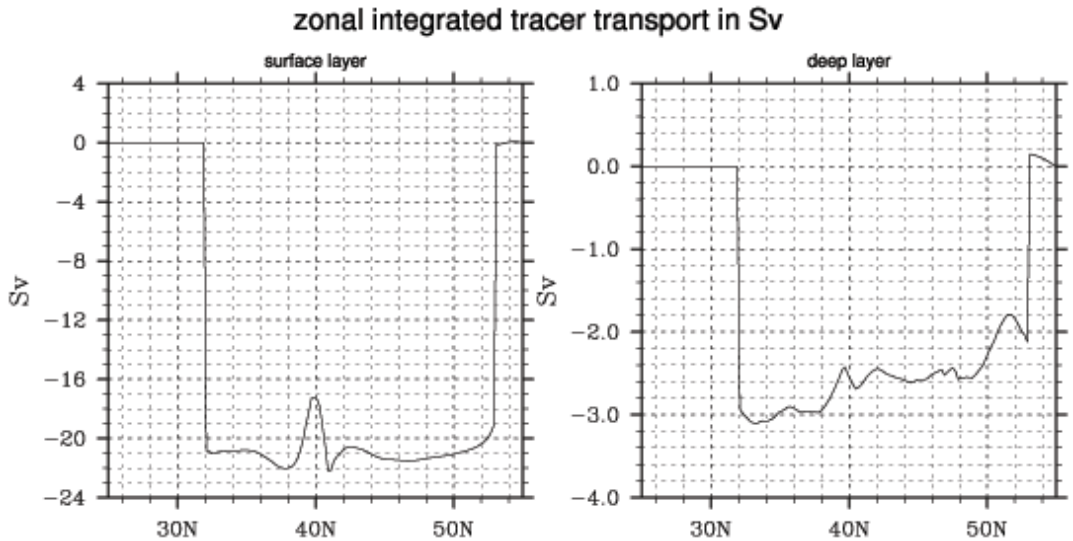

Figure 11 – zonal integrated tracer transport in Sverdrup for surface layer (left) and deep layer (right).

5.2 Tracer concentration in 2 gyres

The pathways of the tracer are also well visible by analysing the tracer concentration in the domain. The five years average statistical equilibrium is presented in Figure 12 and Appendix C shows snapshots of the 25 years of spin up time. The figures in the appendix confirm the analysis that most of the tracer is in the deep layer transported via the interior around the jet and only a small fraction of tracer is transported via the deep western boundary current.
The concentration of tracer in Figure 12 shows for the surface layer the subpolar gyre is quite uniformly filled with tracer, a higher concentration at the western boundary due to the southward western boundary and a lower concentration in the east, due the northward interior flow. For the subtropical gyre there is a narrow track of zero concentration due to the northward western boundary current originating from the removal area, in the interior the concentration is higher due to mixing with the subpolar gyre across the jet.

For the deep layer the concentration is largest in the interior stretching south from the tracer injection zone. Especially in the east of the subpolar gyre a large limb of tracer is advected southward. South of the jet in the subtropical gyre the tracer confines to the western boundary due to the recirculation flow from the jet and further south due to the deep counter current that originates by the secondary recirculation cell.

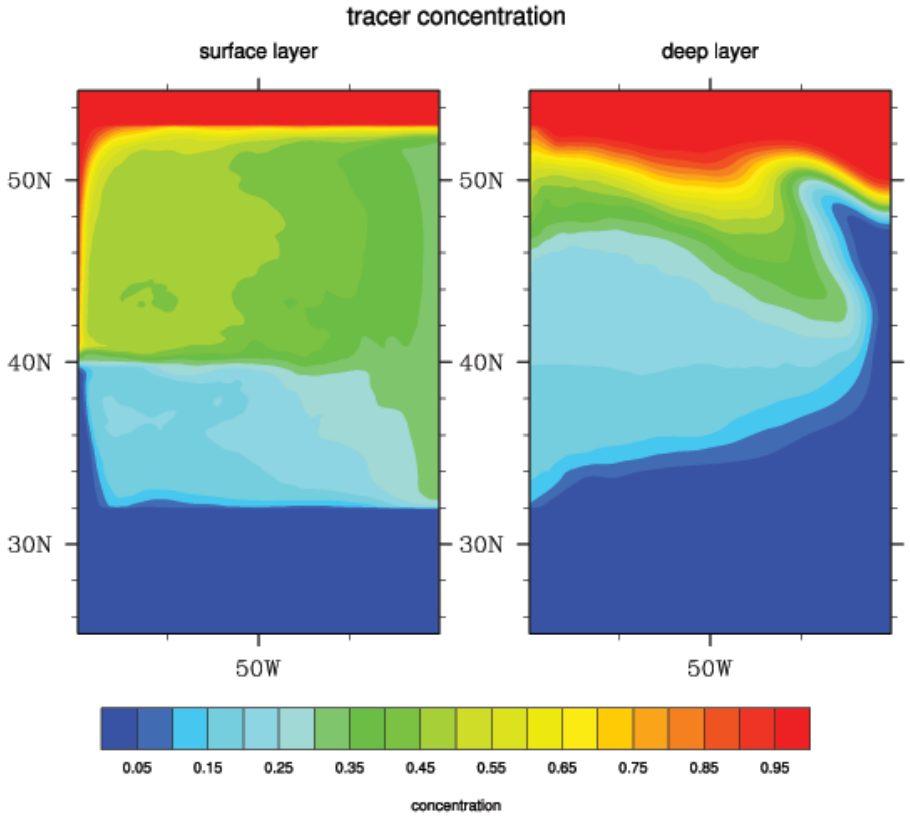

Figure 12 - Tracer concentration for the surface (left) and deep layer (right).

The map in Figure 12 shows a quite strong gradient in concentration between the two gyres of the surface layer due the eastward jet. This gradient is also well visible in the zonally integrated plot of tracer concentration as shown in Figure 13. In the subpolar gyre the concentration is 45% which decreases to 23% by a strong gradient at the location of the eastward jet. However for

the deep layer there is a strong gradient in the north of the subpolar gyre where the tracer is injected, so apparently there is a barrier from tracer to directly advect into the secondary recirculation flow. However at 46°N this strong gradient reduces to a smaller gradient and does not seem to be influenced by the eastward jet as a barrier, while it is for the tracer in the surface layer.

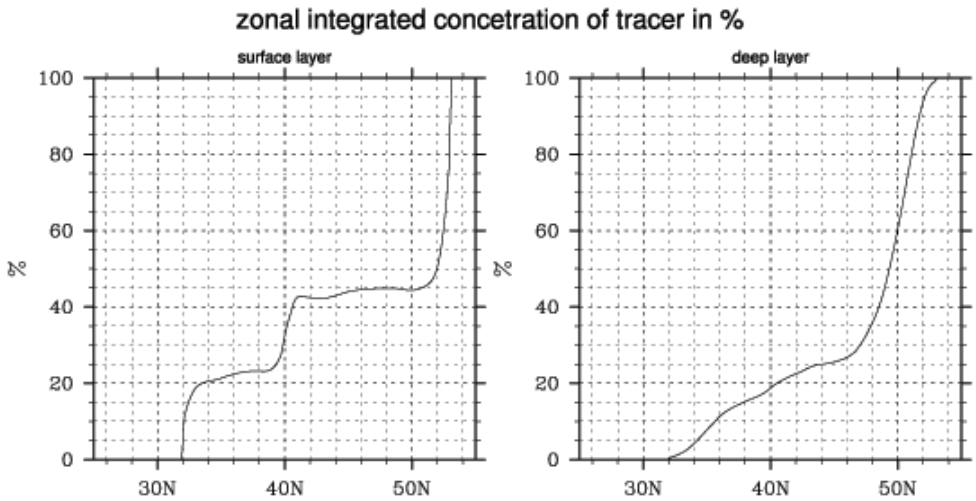

Figure 13 - Zonally integrated tracer concentration reducing in steps for the surface layer (left) while a smoother reduction for the deep layer (right).

5.3 Volume and tracer transport in 4 gyres system

As is described in the introduction of this chapter the North Atlantic Deep Water can be found down to the South Atlantic Ocean. That means that the tracer, apart from an eastward jet, also should be able to cross a westward jet. In this chapter a rather theoretical analysis will be done to test to what extend the tracer can be transported over a 4 gyre system with westward jet which is only wind-driven.

In this experiment the same approach is used as for the previous model experiment, except for this case a 4 gyres system is analysed. The size of the gyres is kept constant, so the domain now ranges from 5° to 65°N. With a wind forcing as given in Appedix D, with maximums of 0.3 Nm^{-2}, the resulting flow velocities are given in Figure 14.

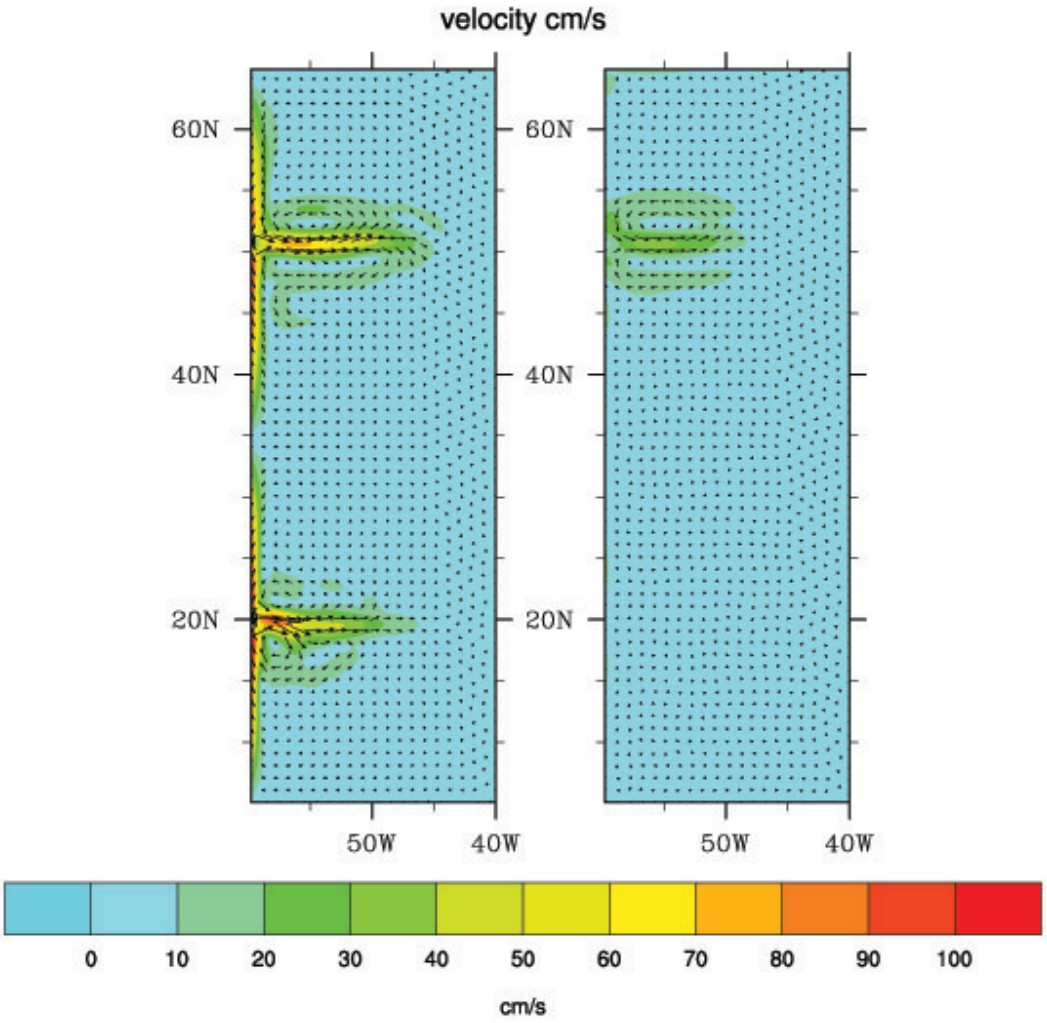

Figure 14 - Flow velocities in cm/s for the surface (left) and deep (right) layer.

For the two northern gyres between 35°-65°N in the domain there is as expected no difference with the two-gyre experiment with an eastward jet at 50°N. At 35°N there is a weak westward jet with a divergence at the western boundary that is hardly visible in the figure. In the domain 5° to 35°N two gyres develop which show, at least for the surface layer, a similar structure as the two northern gyres. Interesting is however that the flow velocity in the southern western boundary currents and the free eastward jet at 20°N are small compared to the two northern gyres. This reduced flow velocity closer to the equator can be explained by the Sverdrup balance as given in equation 16. The value of β increases as latitude decreases, so the meridional velocity, v, has to decrease in order to balance the wind curl. With lower velocities in the western boundary currents the convergent eastward jet at 20°N has a lower flow velocity than the eastward jet at 50°N.

The smaller flow velocities also affect the eddy kinetic energy and thus the meridional volume transport as is shown in Figure 15. In the two most northern gyres the volume transport gives similar results as the results of Figure 9. For the two southern gyres the flow in the surface layer is quite similar as to those for the northern gyres, but for the deep layer some interesting differences appear.

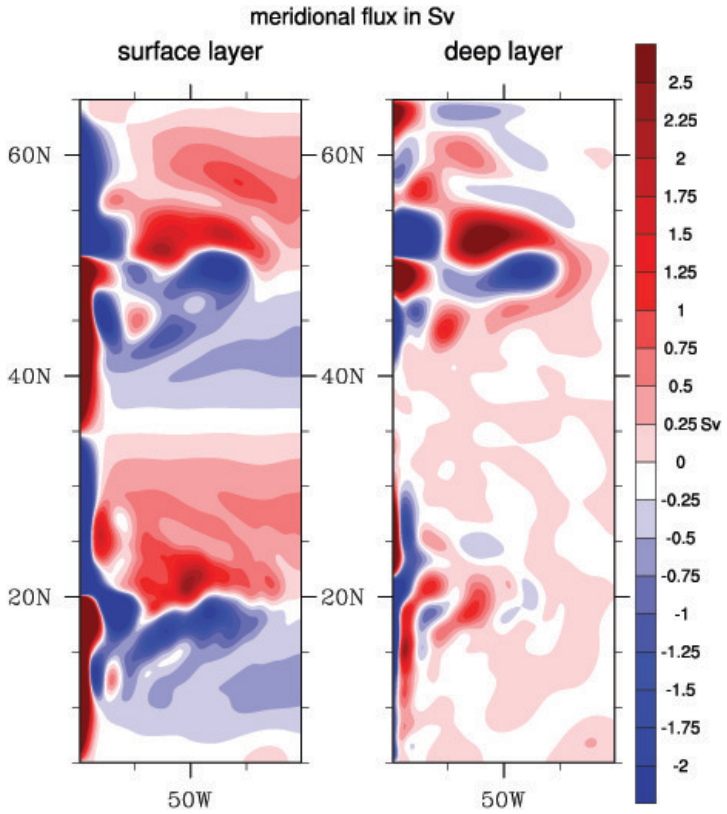

Figure 15 - Meridional volume transport in Sverdrup for the surface (left) and deep layer (right).

In the deep layer there is a narrow but clear northward western boundary counter current over the total gyre length, so from 22°N to 35°N, and south of 22°N a clear southward western boundary current. For both boundary currents this is a counter current compared to the surface layer. Also the free eastward jet is smaller and less extended in eastward direction. The recirculation cells in the deep layer at lower latitudes are more stretched in meridional direction than at higher latitudes. This can be explained by the eddy kinetic energy and the interface height in Figure 16. The interface height displacement is smaller than for the 2 northern gyres, reducing the gradient and the instability. As a result the instability is confined to the jet area and so there are no secondary cells, stretching the boundary current over the total meridional domain of the gyre.

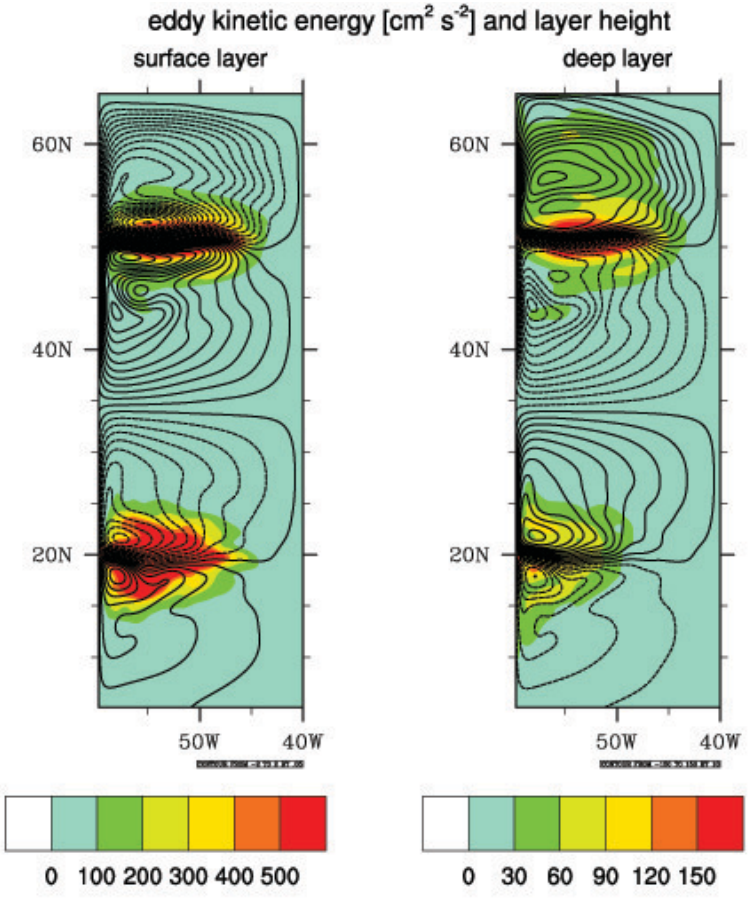

Figure 16 - Eddy kinetic energy and the contour lines of the change in surface height ranging from -2 to 2 meter by 0.05m intervals (left) and change of interface depth ranging from -100 to 100 meter by 10m intervals (right) for a 4 gyre system.

One of the interesting aspects in this analysis is the free westward jet at 35°N. Given the results in Figure 15 there is hardly any meridional volume transport crossing the westward jet. This crossing of the jet however can be better analysed by the use of a tracer.
In this model experiment the tracer is added to the domain at 63°-65°N and removed south of 12°N resulting in the meridional tracer transport maps as given in Figure 17. These results show that for the surface the northern two gyres give the expected and similar result as in Figure 10. The figure immediately shows that the transport of tracer crossing the westward jet is quite difficult. Only a small fraction of tracer is advected southward in the surface layer by the western boundary current from 35° to 20°N. Apparently the westward jet is a barrier and no mixing will take place between the two Sverdrup gyres.
In the deep layer the recirculation cells advect the tracer southward; in the subtropical gyre the deep counter current advects the tracer southward. However here the transport ends, the westward jet has not enough velocity to create circulation cells to connect the circulation cells induced by the eastward jets.

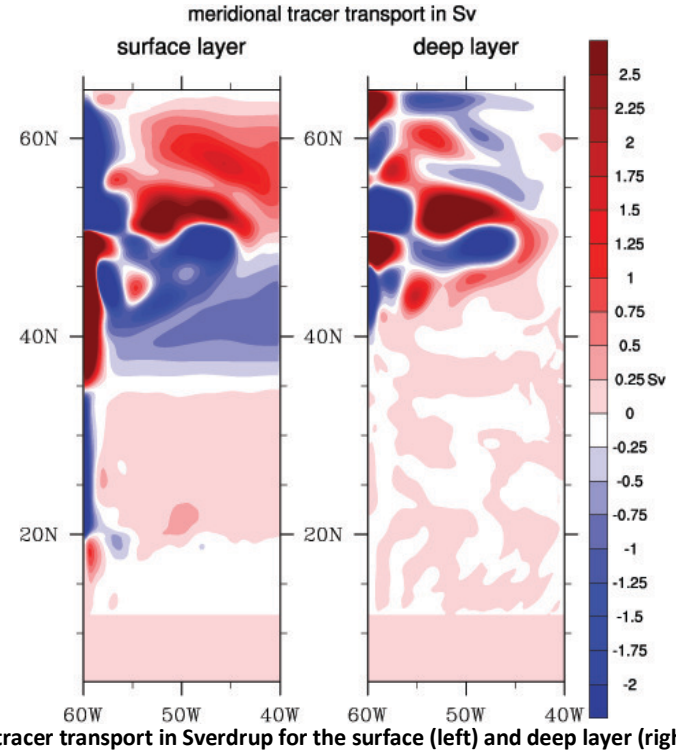

Figure 17 - Meridional tracer transport in Sverdrup for the surface (left) and deep layer (right).

In order to get a better idea about the southward transport, Figure 18 shows the 5 year average tracer concentration during the statistical equilibrium and Appendix E show the snapshots over a period of 60 years. For the surface layer this map shows a clear barrier at the location of the westward jet. For the deep layer the transport of tracer ends at the deep counter current in the south of subtropical gyre.

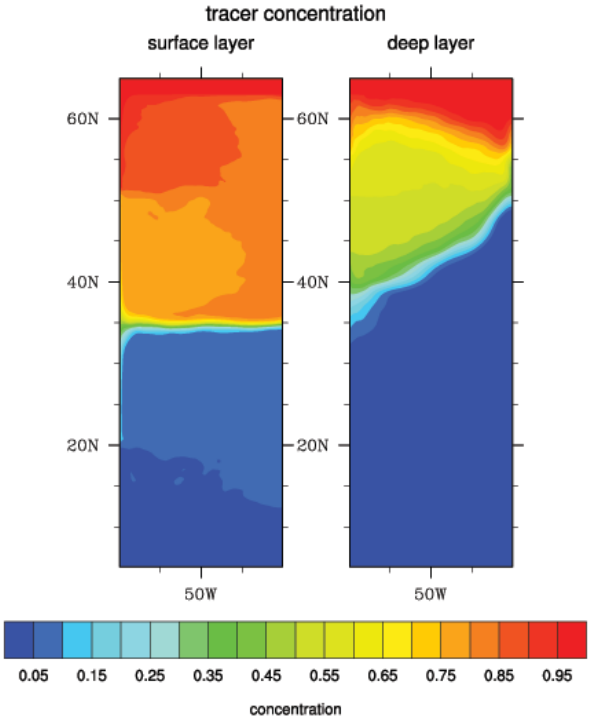

Figure 18 - Tracer concentration for the surface (left) and deep layer (right).

Figure 19 shows the zonal integrated concentration of tracer. In the surface layer the eastward jet is now a smaller barrier compared to the case with the 2 gyres as now there is no removal of tracer in this subtropical gyre. The plot shows a sharp gradient in concentration at the location of the westward jet (35°N) as the concentration drops from 82% to 8%. For the deep layer the end of the deep counter current at 40°N is the end of the tracer transport. Only a very small fraction of 2-3% is able to cross the latitude of 30°N. The next paragraph is dedicated to the transport of tracer crossing jets.

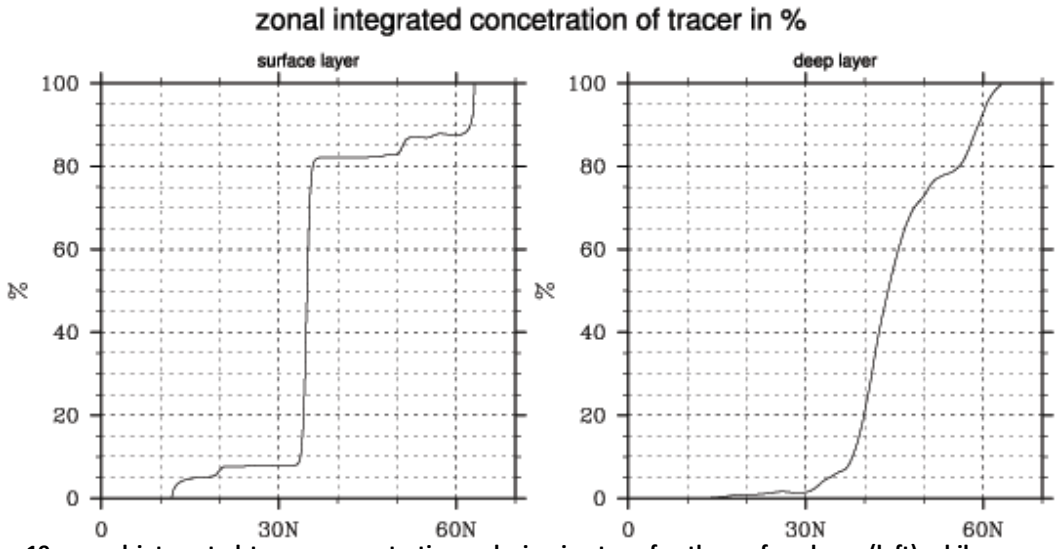

Figure 19 - zonal integrated tracer concentration reducing in steps for the surface layer (left) while a smoother reduction for the deep layer (right).

5.4 Analysis of barriers by eastward and westward jets

The crossing of tracer over a barrier is associated with the potential voriticity (Q). Potential vorticity is related to the Coriolis parameter f, shear (ζ) and layer height h.

$$\frac{\zeta + f}{h} = Q \tag{22}$$

The Coriolis parameter is increasing over higher latitudes and so will the PV, at the location of the jets there is shear so here the PV will have an additional increase. This is visible in Figure 20 (surface) layer shows the zonally averaged PV over the domain, showing an overall increasing value of PV and at locations 50°N and 20°N the two strong eastward jets are located showing a strong PV front.

Apart from the shear also the gyres influence the PV near the jet. In the subpolar gyre there is a counter-clockwise circulation advecting PV in southward direction at the western boundary, in the subtropical gyre the circulation is clockwise advecting PV in northward direction. This advection of PV increases the gradient near the location of the jet creating PV fronts. These PV jumps can be strong barriers preventing tracer to cross the barrier (Esler, 2008).

The surface layer has strong eastward jets and a gyre structure and therefore large PV jumps (Figure 20). In the deep layer the eastward jets have a lower velocity and instead of the gyre structure the layer is organised by recirculation cell which provide a mixing of the PV creating a decrease of PV gradient at the location of the jets at 20°N and 50°N.

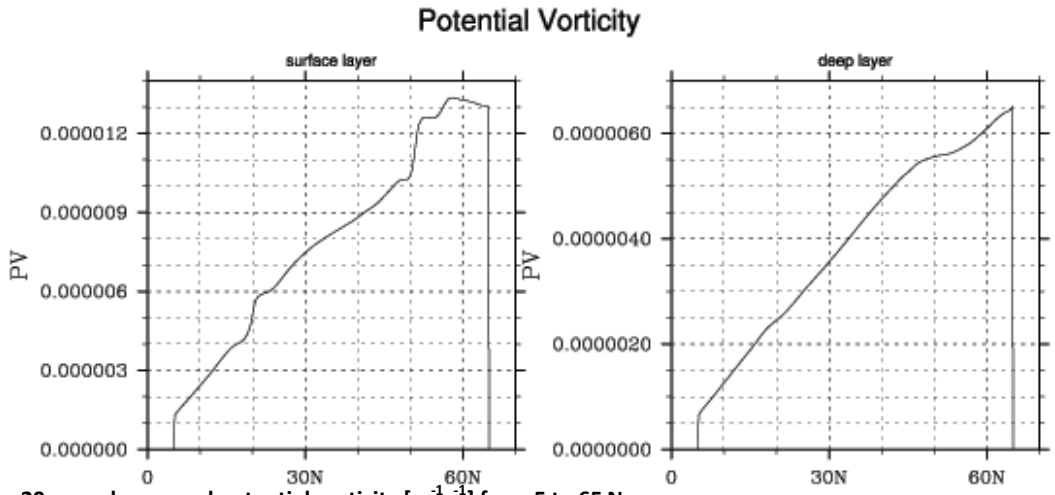

Figure 20 - zonal averaged potential vorticity [$m^{-1}s^{-1}$] from 5 to 65 N.

The key to overcome these barriers is sufficient barotropic and baroclinic instability which generate enough eddy kinetic energy to mix the jet. Therefore the figure of eddy kinetic energy (Figure 16) gives a good insight in the transport across the jet. In the two northern gyres there is a lot of instability providing enough eddies to transport the energy to deep layer and to transport the tracer to the second gyre. At 35°N there is only small vertical and horizontal shear which creates not enough instability to create eddy kinetic energy and therefore not enough mixing to cross the westward jet. At 20°N there is again eddy kinetic energy but no tracer to cross this jet. This result show that the instability is not only a requirement for deep layer transport, it also determines the (southward) transport of tracer across a jet.

6 Wind-driven circulation and the meridional overturning circulation

In this chapter the volume transport in a 2-gyre system is analysed in HIM in order to analyse whether an Atlantic-meridional-overturning-like circulation can be established in the model and which aspects of the MOC can be found in the model. The last part is carried out by comparing the results of the 2-gyre experiment with the results of measurements.

6.1 Measurements of RAPID

In this chapter the model results are compared with the results of measurements. These measurements have been carried out in order to analyse the variability of the MOC and the possible reducing strength of the MOC by the climate change. The measurements are carried out by the Rapid climate change programme (RAPID) (Rayner et al., 2011) and provides insight in the variability of the deep western boundary current east of Abaco (Bryden et al., 2005), (Lee et al., 1990) and the zonally integrated volume transport in the Atlantic Ocean at 26.5°N (Cunningham et al., 2007). The measurements consist of three elements, the Gulf Stream transport, the Ekman transport and the mid-ocean transport.

The induced voltage on submerged telephone line across the Florida Strait records the Gulf Stream transport. These records are calibrated with direct measurements what provides accurate measurements of the Gulf Stream transport (Rayner et al., 2011). The Ekman transport is not measured but derived from satellite-based measurements of the wind stress, which integrated over the basin width is used to calculate a transport. The mid-ocean transport measurement is conducted by several moorings east of Abaco (26.5°N), obtaining pressure and density differences between east and west (see Figure 21) which determine a baroclinic and barotropic transport (Rayner et al., 2011).

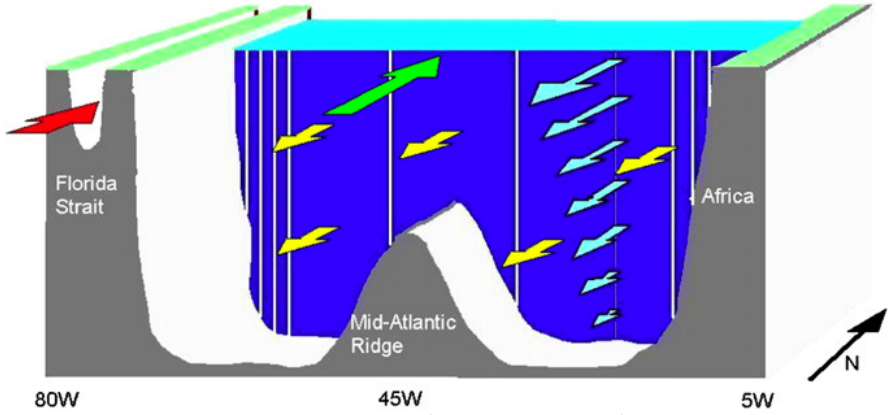

Figure 21 - Schematization of MOC monitoring at 26.5N (Rayner et al., 2011).

Across the Atlantic Ocean at 26.5°N the net mass balance is zero and as a result the three elements measured in the Rapid programme should add up to zero. In the analysis (Rayner et al., 2011) the elements in the upper ocean do not added up the zero and the remaining is considered to be the Meridional Overturning Circulation (MOC). This MOC is flowing northward in the upper layer and is compensated by a southward flow in the deep layer. It is here significant to note that in the RAPID programme the upper layer is considered to a depth of 1100 meter. The results of 4 years of measurements and the resulting MOC are shown in Figure 22.

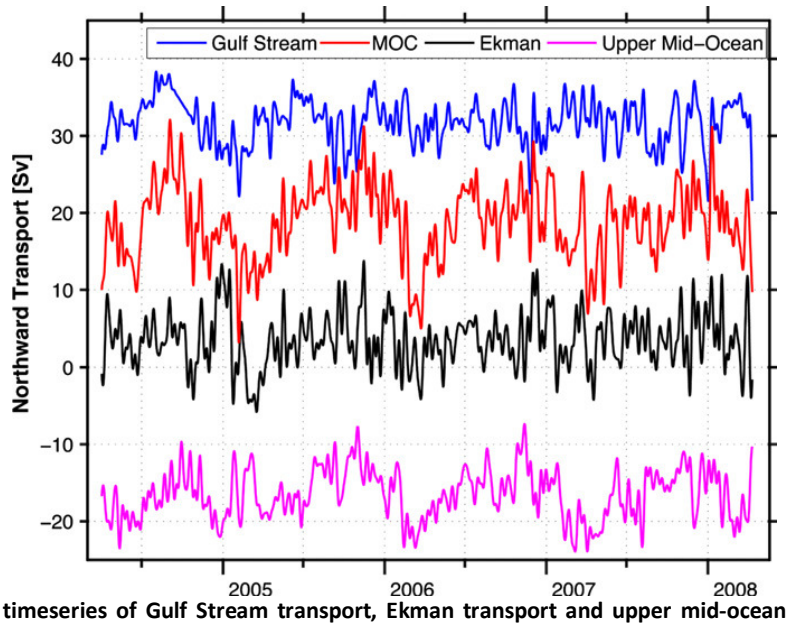

Figure 22 – Daily timeseries of Gulf Stream transport, Ekman transport and upper mid-ocean transport for the period 2 April 2004 – 10 April 2008. (Rayner et al., 2011)

The results show a Gulf Stream transport of around 30 Sv, a fluctuating Ekman transport with an average transport around 3 Sv and a Mid-Ocean transport of around 16 Sv and all three elements show a seasonal cycle. The sum of the three transports is defined as the MOC of around 18 Sv with a summation of the fluctuations.

6.2 Modelling volume transport over 34N with time variance

In order to make a comparison with the observations the seasonal cycle of the wind forcing is implemented in the model. In the previous experiment the wind forcing had a maximum of 0.3 N m^{-2}. In this experiment the wind forcing changes each month (Figure 23) with a yearly averaged maximum forcing of 0.3 N m^{-2}.

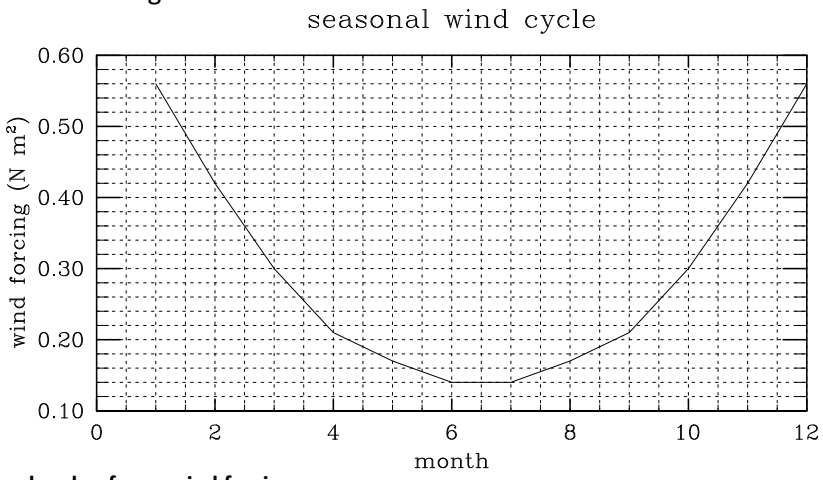

Figure 23 - Seasonal cycle of max wind forcing.

Before the comparison is made between the model results and the measurement first several aspects of the meridional volume transport at this cross section are analysed. The results of chapter 4 and 5 have shown that in the deep western boundary current of the subtropical gyre the southward transport occurs. This is also the location which is well analysed by the RAPID

programme at 26.5°N. The location of 26.5°N is in the model comparable with 34°N as it is more or less in the middle of the gyre and characterised by the deep counter current and the recirculation.
The varying wind forcing results in a seasonal cycle in the meridional volume transport. The result of volume transport is integrated over the total width of the domain as presented in Figure 24.

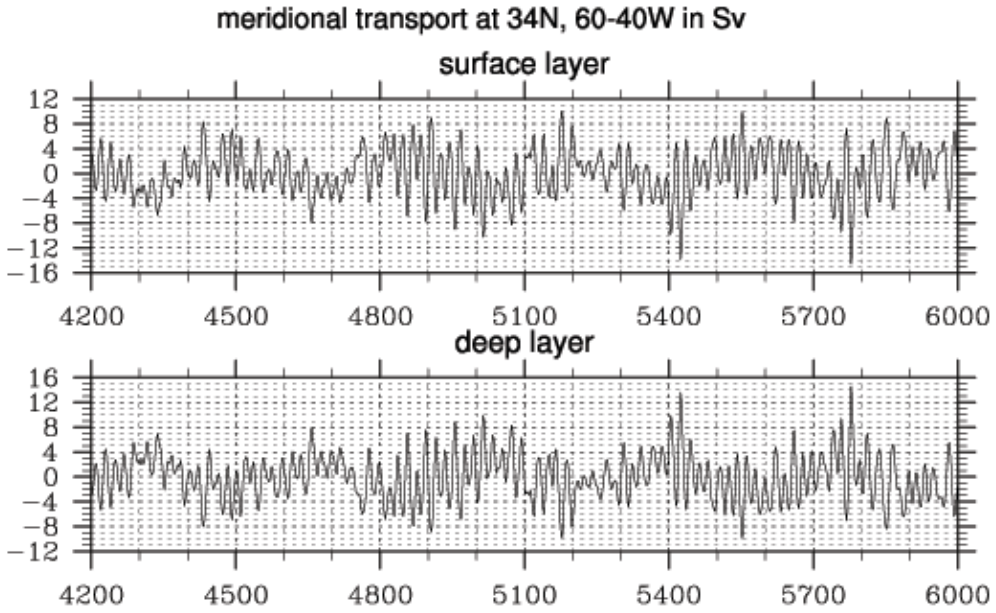

Figure 24 – Meridional volume transport in the surface and deep model layers integrated over the total width of the domain (60°W – 40°W). The surface layer and deep layer are by definition each other mirror image.

The plot shows the seasonal cycle of a 5 years period. The days 4320, 4680, 5040, 5400 and 5760 can all be considered as the 1st of January of successive years and these moments all coincide with maxima in southward transport in the surface layer and maxima of northward transport in the deep layer. The changing depth of the interface compensates the difference in northward and southward transport between the layers. The figure shows that the meridional volume transport fluctuates around zero, as over the time average there is no resulting northward or southward transport for each layer.

Figure 25 shows the zonal integration of the western boundary current ranging from 60° to 55°W. Again these results show the seasonal cycle induced by the monthly wind forcing but it also shows variability on a much shorter time scale. The amplitude of the variability is especially in the second half of the period quite large. For the surface layer this figure shows the western boundary current with on time average a northward transport of around 40 Sverdrup. For the deep layer the transport is only 3 Sverdrup southward because over the domain of 60°-55°W the integral is over both the deep counter current and the northward recirculation.

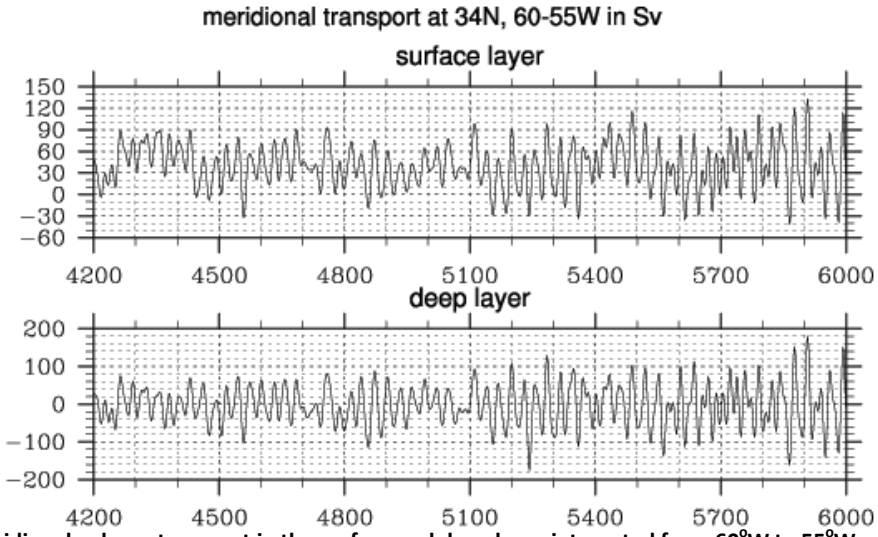

Figure 25 – Meridional volume transport in the surface and deep layer integrated from 60°W to 55°W.

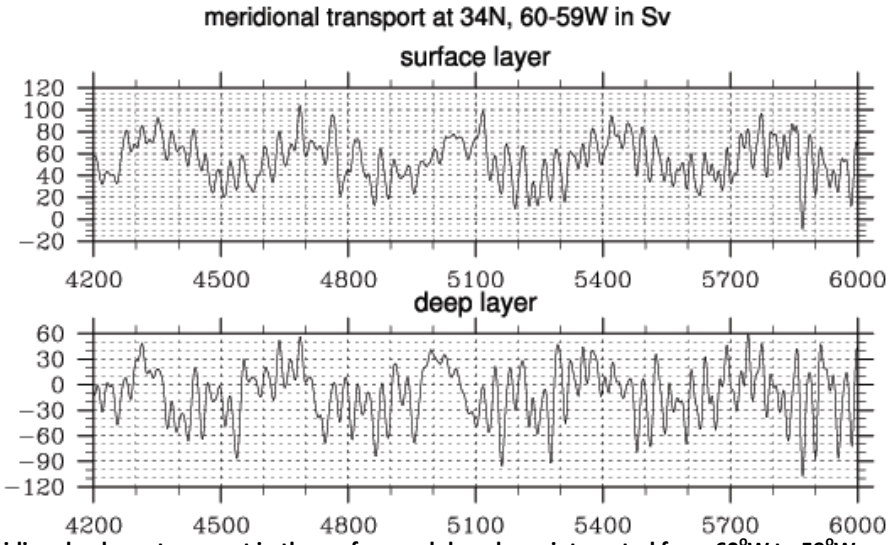

Figure 26 - Meridional volume transport in the surface and deep layer integrated from 60°W to 59°W.

In order to analyse only the deep counter current, Figure 26 shows the zonal integration over 60°-59°W containing only the deep counter current in the deep layer. As a result the surface layer has now a northward transport of 54 Sverdrup and the deep layer a southward transport of 10 Sverdrup. The result show a clear seasonal cycle and the short timescale variability has decreased, compared to Figure 25. This shows a more constant boundary current than the recirculation. In the paragraph 6.4 the short timescale variability is further analysed.

Figure 27 shows the time averaged cumulative meridional volume transport starting from 60°W. For the surface layer the transport is northward in the western boundary current with a maximum of 54 Sverdrup and in the interior the transport is Southward and reaches zero at 40°W, meaning over the whole domain there is no net northward or southward transport. This is due to the fact that in the HIM model the mass balance is solved for each layer. This means there can by definition no MOC-like circulation develops in the HIM model.

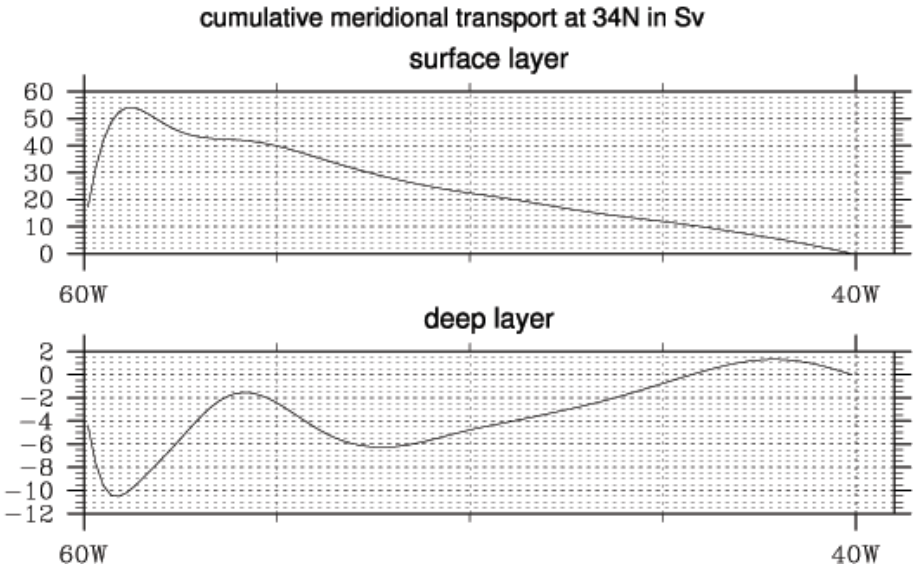

Figure 27 - cumulative meridional volume transport with seasonal cycle

For the deep layer there is also no net transport. It shows the deep counter current that reaches a maximum of just over 10 Sverdrup in southward direction. Then there is a quite significant recirculation that reduces the cumulative transport to 2 Sverdrup. In the interior from 57^{o}W to 53^{o}W there is some additional southward transport and further east the compensating northward transport with a small southward transport at the eastern boundary.
Interesting to see is the effect of the wind variation compared to the results without the seasonal cycle as Figure 28 shows. Without wind variation the southward deep counter current reaches a maximum of 17 Sverdrup, the northward recirculation reduces the southward flow to 6 Sverdrup and in the interior there is the remaining compensating northward transport. These two results show the effect of varying wind forcing; the time averaged volume transport for the seasonal cycle is not the same as the volume transport with a constant averaged forcing. The strength of the increased and decrease deep boundary counter current due to the varying wind forcing is over 5 years averaged smaller, which results into a different balance over the domain width.

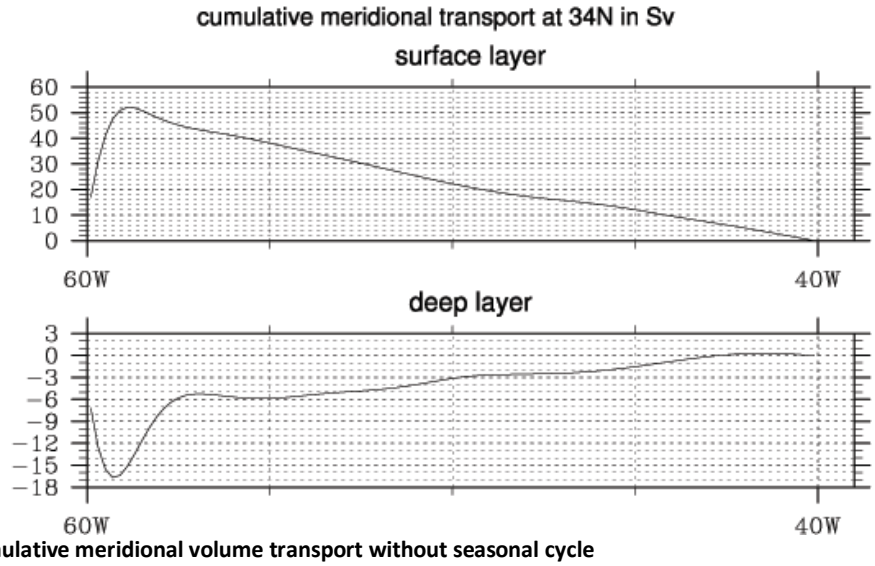

Figure 28 - cumulative meridional volume transport without seasonal cycle

6.3 Comparison of RAPID array with model results

The results of the two previous paragraphs show some interesting results. The RAPID array shows there is a net northward transport in the surface layer (z<1100m.). This net northward transport is called the Meridional Overturning Circulation (MOC) and has to be compensated by a southward transport in the deep layer in order to achieve a net zero transport over the total cross section (deep and surface layer).
In HIM there is for both the surface and deep layer no net meridional transport. This is on one side a limitation of the model as there is no vertical transport between the two layers. One the other hand the wind driven gyres do not allow an overturning circulation. The Sverdrup flow creating the gyre structure solves the net wind-driven transport in the horizontal plane and so do the recirculation cells in the deep layer.
Given these results it is however interesting to "apply" the RAPID programme in the HIM model and analyse the individual elements that create the MOC.

In the RAPID programme the Gulf Stream is obtained by direct measurements, this will also be done in the model taking the integrated transport in the surface layer from 60°W to 57°W.

The Ekman transport is calculated by:

$$T_{Ek} = -\int \frac{\tau_x}{\rho f} dx \tag{23}$$

The mid-ocean transport can be computed by the difference in pressure (barotropic) and density (baroclinic) between east (40°W) and west (57°W). The equation for the baroclinic transport reads as follows:

$$T_{baroclinic}(z) = -\frac{g}{\rho f}\int_{Zref}^{0} [\rho_E(z) - \rho_W(z)]dz \tag{24}$$

And the equation for barotropic transport is:

$$T_{barotropic} = \frac{Hg}{f}(\xi_E - \xi_W) \tag{25}$$

These two transports integrated for the upper ocean (depth 1100 meter) gives the upper ocean transport.
However in the RAPID array the sea surface height is not measured so the barotropic transport cannot be calculated. Therefore the following balance is considered as there is no net transport in the ocean:

$$T_{Gulf\ Stream} + T_{barotropic} + T_{baroclinic} + T_{Ekman} = 0 \tag{26}$$

Based on this equation the $T_{barotropic}$ can be determined. This transport is considered to be eventually distributed over the ocean's cross section.
To determine the Meridional Overturning Circulation the upper ocean (depth <1100 meter) is considered, this is determine by the following balance:

$$T_{Gulf\ Stream} + \int_{-1100}^{0} T_{barotropic} + \int_{-1100}^{0} T_{baroclinic} + T_{Ekman} = MOC \tag{27}$$

The summation of the baroclinic and barotropic transport for the upper ocean is called the (upper) mid-ocean transport $T_{mid\text{-}ocean}$. The transports and resulting MOC were presented in Figure 22.

In this study the HIM model provides the opportunity to calculate the barotropic transport, as described by equation 25, because the surface height can be obtained in the HIM model. Again transport is taken for the upper 1100 meter and the barotropic and baroclinic transport combined is the mid-ocean transport. The result is presented in Figure 29.

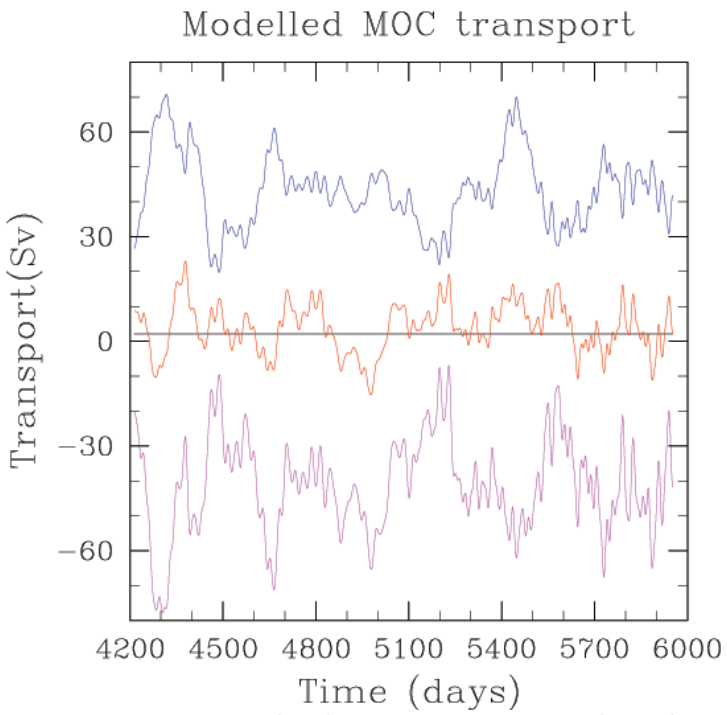

Figure 29 - Volume transport of the Gulf Stream (blue), the mid-ocean transport (purple), Ekman transport (black). The sum of these three provides the MOC transport (red).

The Gulf Stream transport has here a time averaged transport of 43.1 Sv, the mid-ocean transport -41.4 Sv, Ekman transport is 2.1 Sv so the resulting MOC has a time averaged transport of 3.9 Sv. This provides an interesting result given the fact that in the HIM model the balance should be zero, as there is no MOC like circulation in HIM. The mid-ocean transport and the Gulf Stream transport are closely in balance with each other, there is only a difference of 1.7 Sverdrup. The reason for this difference is due to the assumption of a constant transport between 57°W and 40°W by the calculation of the barotropic and baroclinic transport. The cumulative transport of Figure 28 however does not show a clear linear line, but a line with some small variations indicating small variations in the transport. The difference from an exact constant transport is most likely this 1.7 Sverdrup.
This result however shows that with this calculation imperfection the balance of zero net transport is closed without the Ekman transport. Given this result there is no reason to take the Ekman transport into account as part of the MOC, as it is the Ekman transport that creates the changing surface and interface gradient. By taking the Ekman transport out of the MOC the MOC reduces to the 1.7 Sv, which is due to calculation. If this is now applied to the measurements and the Ekman is taken out of the RAPID array this will give the transport as presented in Figure 30.

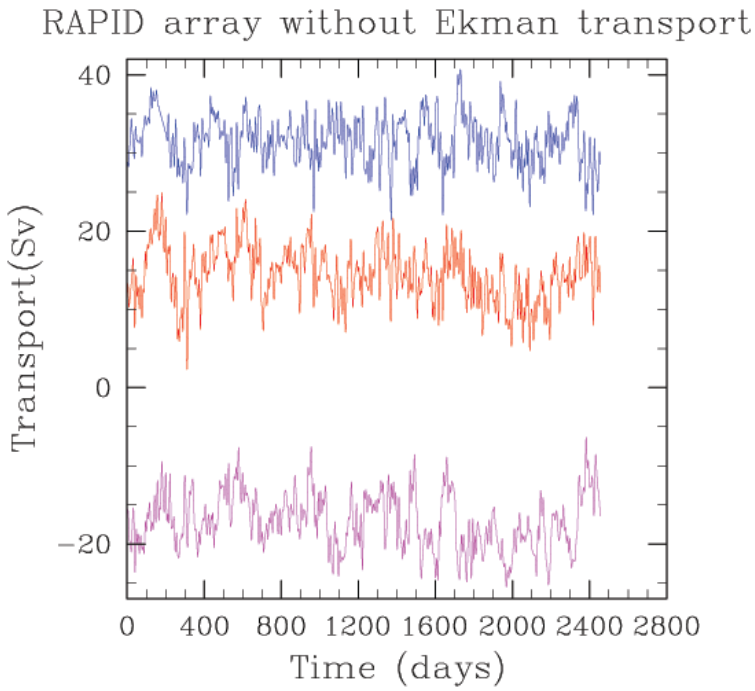

Figure 30 - Gulf Stream transport (blue), mid-ocean transport (purple) and the resulting MOC (red) if the Ekman transport is not taken into account.

The Gulf Stream transport is time-averaged 31.6 Sv, the mid-ocean transport is -17.1 Sv and the resulting MOC is now 14.4 Sv. This means the MOC is reduced by 3 Sv as this was the contribution of the Ekman transport. Not only is the time averaged transport of the MOC reduced, the variability has decreased as well. This is because the Ekman transport added a lot of timescale variability to the MOC. The standard deviation reduced from 4.7 Sv with the Ekman transport to 3.6 Sv without Ekman transport. The time variability is further analysed by the frequency analysis in the following paragraph.

6.4 Frequency analysis

The results of the two previous paragraphs showed short timescale variability. In this paragraph the timescales are analysed by the use of an energy-spectra and are compared to spectra of the observed MOC (Cunningham et al., 2007).

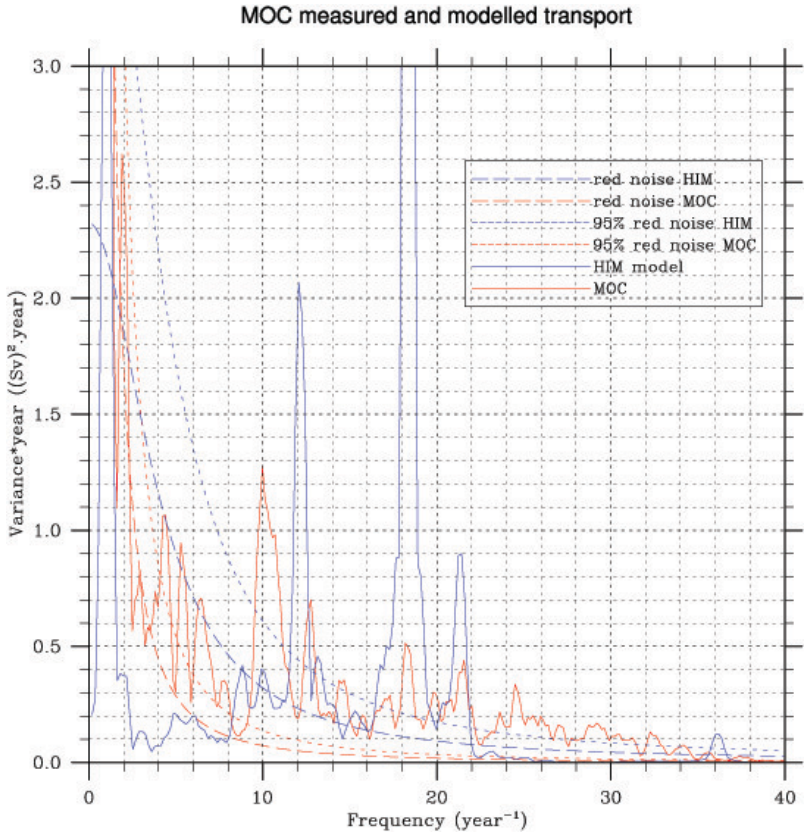

Figure 31 – Spectral analysis of measured MOC and meridional transport in HIM. The dashed and dotted lines show the red noise and its confidence interval.

Figure 31 shows in blue the variance of the meridional volume transport integrated at 34°N over the total width of the domain. The plot shows a large peak at a frequency of 18 per year, this is the variability as observed in Figure 24. This variance is most likely the frequency related to the basin mode.
The angular frequency of the basin mode can be calculated by:

$$\sigma_0 = -\frac{\beta k}{k^2 + l^2} \tag{28}$$

Using this equation leads to a wave length of 5 km which is however quite small typical wave length of eddies (Gill et al., 1974).
Apart from this frequency the model results show some other significant frequencies at 1 per year, 12 per year and 21 per year. The first and the second are respectively the yearly and monthly cycles that are forced by the varying wind. The short scale variability is a typical frequency induces by the eddy activity.
Interesting is that these four significant peaks also appear in the energy spectra of the measured MOC. In the measured MOC there is a 2-yearly variability and a strong 10 per year variability. The short timescale variability that is observed in the model result is also there in the measured

MOC (18 and 21 per year). This is an indication that the MOC is influence by a (wind) forcing creating variability with a similar frequency.
An analysis of the frequencies of the individual elements showed that most of the energy in the range of 4-8 per year is due to the Ekman transport. In the previous paragraph it was concluded that the Ekman transport should not be taken into account considering the MOC. Therefore Figure 32 shows the energy spectrum for the MOC that is only based in the Gulf Stream transport and the mid-ocean transport.

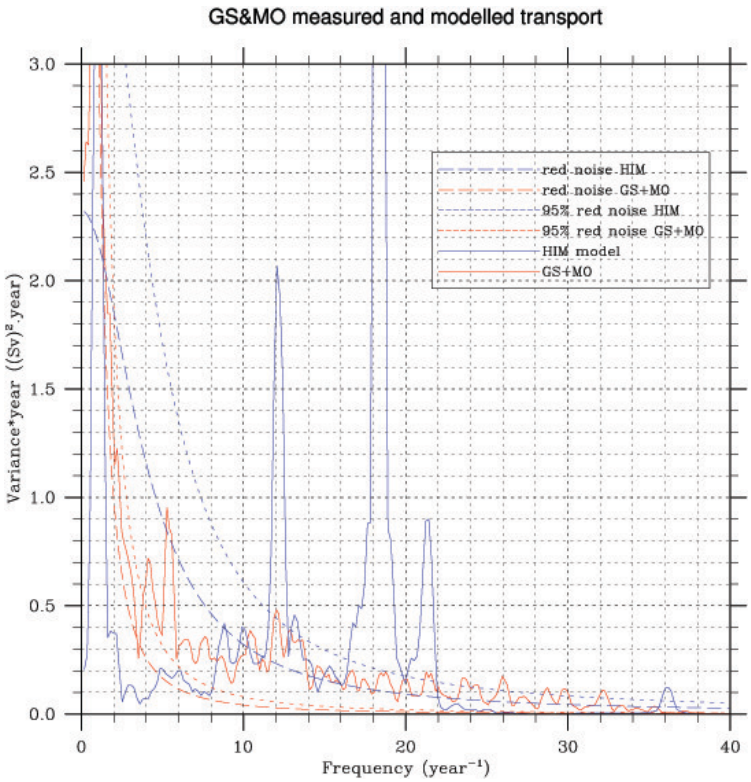

Figure 32 - Spectral analysis of the MOC, based on only the Gulf Stream and mid-ocean transport, and the meridional transport in HIM. The dashed and dotted lines show the red noise and its confidence interval.

The result shows there is less variability in the MOC as this was caused by the Ekman transport. This result is not really more in accordance with the HIM model. In the range of 4-8 per year has a lot of variability is removed. For these frequencies there is more accordance between the measurements and the model results. The variability at 10-12 and 18-21 per year has decreased as well, which reduces also the relation between the model and measurements.

7 Discussion and conclusion

In this final chapter the conclusion of this study is given answering the three research questions. In additional the discussion is given analysing two aspects which might influence the model results.

7.1 Conclusion

To what degree does the wind forcing provide a gyre structure created by eddies in the deep layer?

The wind forcing drives the surface layer and creates eddy kinetic energy that drives the deep layer with a gyre structure. The eddy kinetic energy drives an eastward jet in the deep layer creating recirculation cells with a deep western boundary current. Further south and north of the jet secondary cells exist with a deep counter current. The deep counter current is thus a result of eddies forcing the deep layer and is not a result of the MOC.

To what extend provides the deep layer a meridional transport of a (NADW-like) tracer?

The deep counter current is considered to be a result of the MOC as it has characteristics of North Atlantic Deep Water. This is because the deep western boundary currents and recirculation cells provide a southward transport of tracer in the deep layer. The subpolar gyre is filled with tracer mainly via the interior, following the southward flow of the recirculation cell. The tracer is transport southward east of the jet following the recirculation cell in order to reach the deep western counter current. The recirculation cells enhance the velocity in the eastward jet, creating conditions for tracer to cross the jet. Due to the absence of recirculation cell near the westward jet, the flow velocity is small and close to zero percentage tracer crosses this westward jet.

Can the wind forcing provide a MOC-like circulation and/or can MOC-aspects/variability be explained by the wind forcing?

A MOC like overturning is by definition not possible to represent in the HIM model as the mass balance is solved per layer instead of over the total basin. However the gyre structures in both the surface and deep layer show a significant horizontal volume transport. The volume transport in the deep layer show secondary recirculation cells which reach quite far east, it is questionable whether these are well measured and interpreted in RAPID measures. A comparison of the model results and the measurements show that the Ekman transport should not be considered as a contribution to the MOC. This reduces the MOC by 3 Sv and decreases its variability. The variability of the measured MOC shows similarities in both energy and frequencies of the modelled volume transport, this relation partly increases if the MOC without Ekman transport is analysed.

The hypothesis stated in the Introduction is not confirmed; there is no evidence that the MOC is wind driven. However the study shows that several elements, which are considered to be part of the MOC, are in fact forced by eddies in the deep ocean which originate from the wind forcing. This study shows that the Ekman transport is not an element that should be taken into account

in determining the MOC, in fact the result of Ekman transport is already taken into account by the Gulf Stream transport and the mid-ocean transport. Nevertheless there is still a significant MOC that by these results cannot be attributed to the wind forcing.

7.2 Discussion

In this paragraph two aspects in the modelling are discussed which influence the model results. The first aspect is the effect of a more realistic land boundaries, this is analysed by modelling the total Atlantic Ocean with its main continental land boundaries, creating a geometry which better represents the Atlantic Ocean.
The second aspect which is analysed is the difference in density between the two layers, during this study the difference was 5 kg m^{-3}. In this analysis this is reduced to 2 kg m^{-3}, a smaller difference will give more interacting between the layers and the result of this on the transport in the deep layer is here analysed.

7.2.1 4 gyre system with land boundaries

As paragraph 5.3 and 5.4 show the westward jet has a low velocity and as a result this jet acts as a barrier in the transport of tracer in the southward direction. In order to analyse whether this low velocity might be influenced by the lack of realistic land boundaries the model experiment is adjusted by the implementation of the continental land boundaries with a maximum wind forcing of 0.3 N m^{-2} based on (COAS, 2012). The domain and wind profile are given in Appendix F. All other model parameters are kept constant and the resulting meridional volume transport is presented in Figure 33.

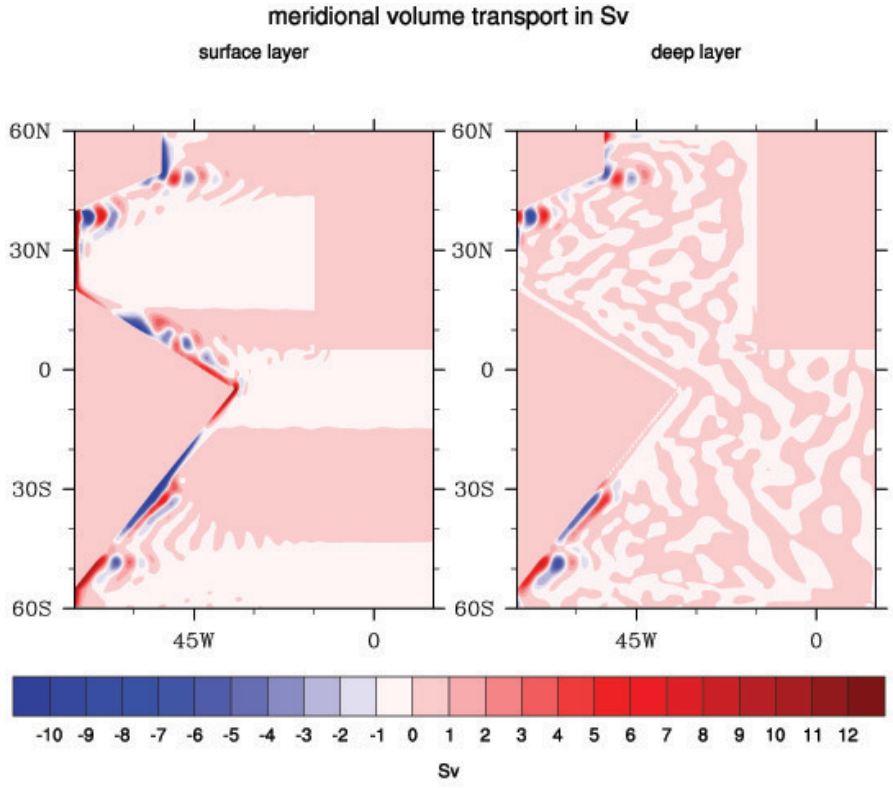

Figure 33 - Meridional volume transport in schematised Atlantic Ocean with contour of continental land boundaries.

The result clearly shows that in the deep ocean layer there is hardly any transport activity at latitudes 30°N to 30°S. At the North coast of South-America there is some motion in the surface layer with eddy kinetic energy (appendix G) but this kinetic energy is not transported to the deep layer. The westward jet would, given the wind forcing, be expected at 15°N and 15°S; these jets are there in the surface layer, but are not unstable enough to create a meridional transport over the domain. In the deep layer these jets are not developed, as there is no eddy kinetic energy to force these. Overall it can be stated that tracer transport can be transported over the eastward jets but westward jets limit the further southward transport of tracer.
The eastward jet at 40°N has changed due to the land boundaries; this is best visible in Figure 34. The figure shows the jet at 40°N with its recirculation cells, the western boundary of the subpolar now extents less south than without the land boundary. This is also the case for the deep layer, while for the subtropical gyre the deep counter current is at is expected location.

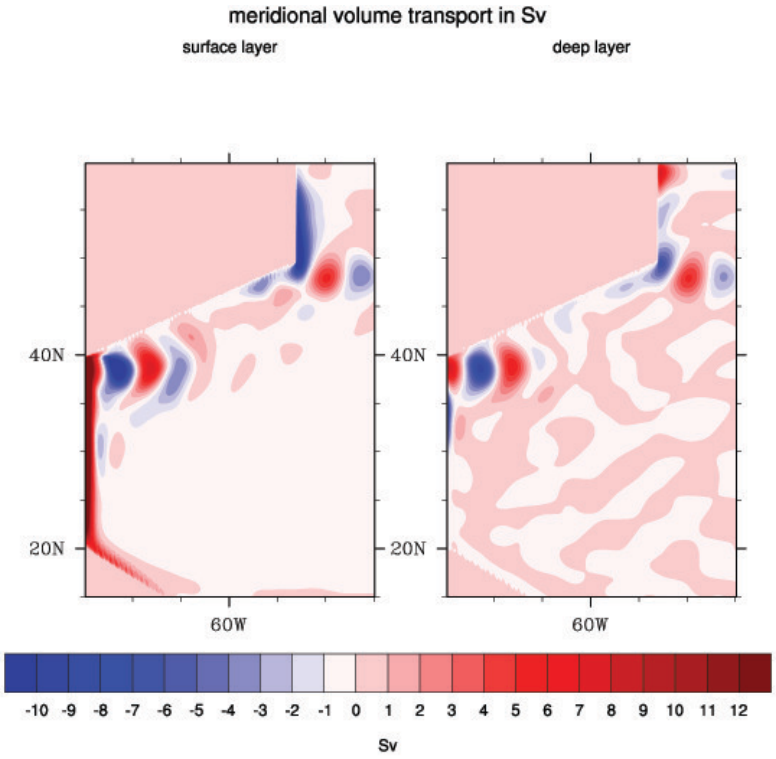

Figure 34 –Zoom in on the eastward jet located at 40°N and the boundary currents

7.2.2 Density difference between layers

In the study so far the surface layer had a density ρ of 1030 kg m^{-3} and the deep layer a density of 1035 kg m^{-3}. In this analysis the density in the deep layer is increased to 1033 kg m^{-3} and the resulting eddy kinetic energy is given in Figure 35.

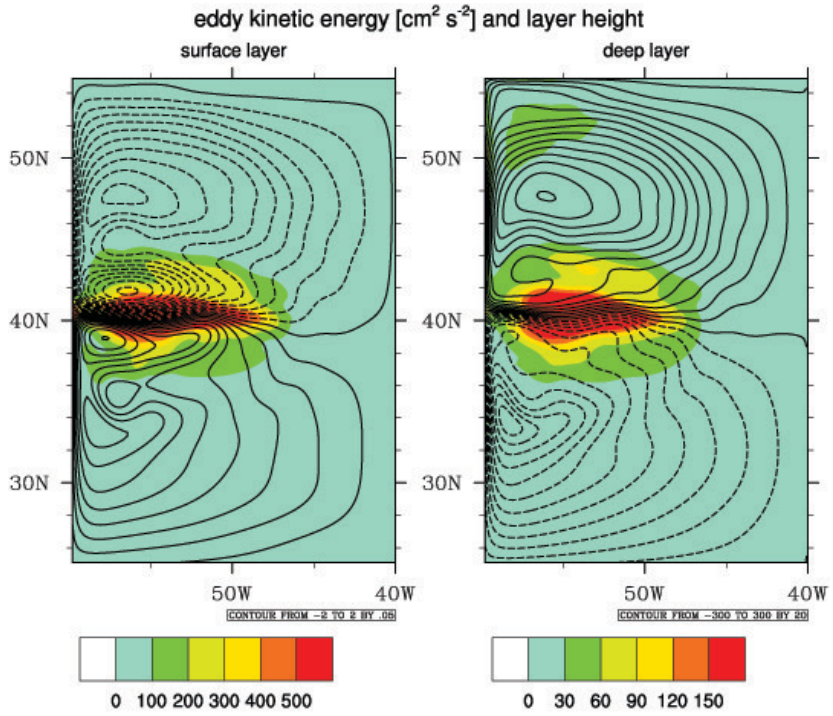

Figure 35 - Eddy kinetic energy and layer height for experiment with a density difference between the layers of 2 kg m^{-3}. For the surface layer the displacement is given from -2 to 2 meter with intervals of 0.05m, for the deep layer the displacement is given from -300 to 300 meter with intervals of 20 meter.

A comparison with Figure 7 shows there is not much difference in eddy kinetic energy compared to the initial set up. There is as expected a large difference with the height of the interface. The interface is now much deeper in the subtropical gyre and much shallower in the subpolar gyre. The smaller difference in density allows for more changes in the interface height. The effect on the meridional transport is given in Figure 36.

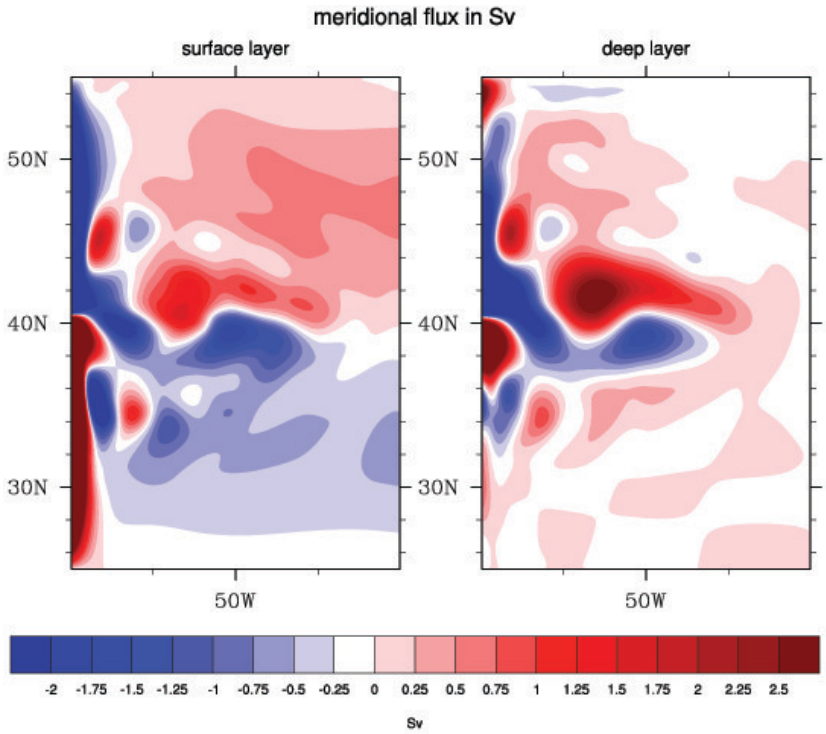

Figure 36 - Meridional volume transport with a smaller density difference between the layers.

The surface layer shows not so much difference with Figure 9. The western boundary currents, the recirculation current and the Sverdrup flow in the interior are all there. For the deep layer there is however an important difference, the secondary cells in both the subtropical and subpolar gyre has largely disappeared and as a result the deep counter currents have almost vanished. This is because the reduced difference in density increased the vertical displacement of the interface but it also decreased the instability and the eddy kinetic energy. This is similar as the result of the two southern gyres of the 4 gyre system; a reduced eddy kinetic energy limits the development of the secondary recirculation cells.

For the subpolar gyre the deep western boundary current is now in southward direction with only in the north a small northward transport. For the subtropical gyre the deep counter current has largely disappeared, there is only a small cell left which does not force a circulation over the total length of the gyre, the deep counter current does not reaches south of 32^{o}N. This result shows that the transport in the deep layer is quite sensitive to the modelling of the layer and its characteristics. It is therefore recommended to do further research on this aspect.

8 References

Biastoch, A., Boning, C. W., & Lutjeharms, J. R. E. (2008). Agulhas leakage dynamics affects decadal variability in Atlantic overturning circulation. [10.1038/nature07426]. *Nature, 456*(7221), 489-492.

Bower, A. S., Lozier, M. S., Gary, S. F., & Boning, C. W. (2009). Interior pathways of the North Atlantic meridional overturning circulation. [10.1038/nature07979]. *Nature, 459*(7244), 243-247.

Broecker, W. S. (1987). The biggest chill. *Natural History, 96*, 74-92.

Bryden, h. L., Johns, W. E., & Saunders, P. M. (2005). Deep western boundary current east of Abaco: Mean structure and transport. *Journal of Marine Research, 63*(1), 35-57.

COAS. (2012). The Scatterometer Climatology of Ocean Winds. Retrieved 14 april 2012, from coas oregon state university http://cioss.coas.oregonstate.edu/scow/

Cunningham, S. A., Kanzow, T., Rayner, D., Baringer, M. O., Johns, W. E., Marotzke, J., . . . Bryden, H. L. (2007). Temporal Variability of the Atlantic Meridional Overturning Circulation at 26.5°N. *Science, 317*(5840), 935-938.

Dijkstra, H. (2008). *Dynamical Oceanography* (Vol. 1). Berlin Heidelberg: springer.

Esler, J. G. (2008). Robust and leaky transport barriers in unstable baroclinic flows. *Physics of Fluids, 20*(11).

Gill, A. E., Green, J. S. A., & Simmons, A. J. (1974). Energy partition in the large-scale ocean circulation and the production of mid-ocean eddies. *Deep Sea Research, 21*, 499-528.

Hallberg, R. (1997). Stable Split Time Stepping Schemes for Large-Scale Ocean Modeling. *Journal of Computational Physics, 135*(1), 54-65.

Holland, W. R. (1978). The role of mesoscale eddies in the general circulation of the ocean-Numerical experiments using a wind-driven quasi-geostrophic model. *Journal of Physical Oceanography, 8*, 30.

Jeffrey, H. (1926). On fluid motions produced by differences of temperature and humidity. *Quart. J. Roy. Meteor. Soc., 51*, 347-356.

Lee, T. N., Johns, W., Zantopp, R., & Schott, F. (1990). Western Boundary Current Structure and Variability East of Abaco, Bahamas at 26.5°N. *Journal of Physical Oceanography, 20*(3), 446-466.

Lozier, M. S. (1997). Evidence for Large-Scale Eddy-Driven Gyres in the North Atlantic. *Science, 277*(5324), 361-364.

Pond, S. Pickard, G.L. (1978). ***Introductory Dynamical Oceanography*** **(second edition ed.). Oxford: Pergamon Press.**

Rayner, D., Hirschi, J. J. M., Kanzow, T., Johns, W. E., Wright, P. G., Frajka-Williams, E., . . . Cunningham, S. A. (2011). Monitoring the Atlantic meridional overturning circulation. ***Deep Sea Research Part II: Topical Studies in Oceanography, 58*****(17–18), 1744-1753.**

Stommel, H. M., Warren, B. A., & Wunsch, C. (1981). ***Evolution of physical oceanography : scientific surveys in honor of Henry Stommel*****. Cambridge, Mass.: MIT Press.**

Wunsch, C. (2002). Oceanography. What is the thermohaline circulation? ***Science, 298*****(5596), 1179-1181.**

Appendix A

```
/*  Specify the physical domain.
#define OMEGA 7.2921e-5          /*    The rotation rate of the earth   */
                                 /*  in s-1.                            */
#define RE 6.378e6               /*    The radius of the earth in m.    */

#define GFS 9.81                 /*    The reduced gravity at the free  */
                                 /*  surface, in m s-2.                 */
#define MAXIMUM_DEPTH 4000.0     /*    The maximum depth of the ocean,  */
                                 /*  in m.  This is required for valid  */
                                 /*  advice from param_suggest.c.       */
#define MINIMUM_DEPTH 1.0        /*    The minimum ocean depth, in m.   */
                                 /*  Anything shallower than this depth */
                                 /*  is assumed to be on land, and all  */
                                 /*  appropriate fluxes are masked out. */
#define GINT 9.81e-3             /*    The reduced gravity of the       */
                                 /*  internal interfaces, in m s-2.     */
                                  /*  GINT may be superseded in          */
                                 /*  initialize.c, but GINT should be   */
                                 /*  the average of all interface re-   */
                                 /*  duced gravities for param_suggest.c*/
                                 /*  to give appropriate advice.        */

/*  Specify the time integration scheme.                                */
#define SPLIT                    /*    Use "#define SPLIT" to use the   */
                                 /*  split time stepping.               */
#define DT 240.0                 /* @  The time step, in s.             */
#define DTBT 30.0                /* @  The barotropic time step, in s.  */
                                 /*  DTBT is only used with the split   */
                                 /*  explicit time stepping.            */
#define BE 0.7                   /* @  BE determines whether the neutral*/
                                 /*  baroclinic time stepping scheme    */
                                 /*  (0.5) or a backward Euler scheme   */
                                 /*  (1) is used.  BE may be from 0.5   */
                                 /*  to 1, but instability may occur    */
                                 /*  near 0.5.                          */
#define BEBT 0.2                 /* @  BEBT determines whether the baro-*/
                                 /*  tropic time stepping uses the for- */
                                 /*  ward-backward timestepping scheme  */
                                 /*  or a backward Euler scheme.  BEBT  */
                                 /*  is valid in the range from 0 (for  */
                                 /*  a forward-backward treatment of    */
                                 /*  nonrotating gravity waves) to 1    */
                                 /*  (for a backward Euler treatment).  */
                                 /*  In practice, BEBT must be greater  */
                                 /*  than about 0.05.                   */

/*Specify the horizontal (along-isopycnal) viscosity.
#define LAPLACIAN                /*    LAPLACIAN is defined to use a    */
                                 /*  Laplacian horizontal viscosity.    */
#undef BIHARMONIC                /*    BIHARMONIC is defined to use a   */
                                 /*  biharmonic horizontal viscosity.   */
                                 /*  BIHARMONIC may be used with        */
                                 /*  LAPLACIAN, and it is automatically */
                                 /*  defined if LAPLACIAN is undefined. */
#define BOUND_KH                 /*    If BOUND_KH is defined, the      */
                                 /*  Laplacian coefficient is locally   */
                                 /*  limited to guarantee stability.    */
#define BOUND_AH                 /*    If BOUND_AH is defined, the bi-  */
                                 /*  harmonic coefficient is locally    */
                                 /*  limited to guarantee stability.    */
```

```
#define KH 500.                 /* @  KH is the Laplacian horizontal   */
                                /*  viscosity, in m2 s-1.  KH is only  */
                                /*  used if LAPLACIAN is defined.      */
#define AH 0.0                  /* @  AH is the biharmonic horizontal  */
                                /*  viscosity, in m4 s-1.  AH is only  */
                                /*  used if BIHARMONIC is defined.     */
#define KH_VEL_SCALE 0.         /* @  The velocity scale which is mult-*/
                                /*  tiplied by the grid spacing to     */
                                /*  calculate the Laplacian viscosity  */
                                /*  if LAPLACIAN is defined, in m s-1. */
                                /*  The final viscosity is the largest */
                                /*  of this scaled viscosity, the Smag-*/
                                /*  orinsky viscosity and KH.          */
#define AH_VEL_SCALE 0.003      /* @  The velocity scale which is mult-*/
                                /*  tiplied by the cube of the grid    */
                                /*  spacing to calculate the biharmonic*/
                                /*  viscosity if BIHARMONIC is defined,*/
                                /*  in units of m s-1. The final vis-  */
                                /*  cosity is the largest of this      */
                                /*  scaled viscosity, the Smagorinsky  */
                                /*  viscosity and AH.                  */
#undef SMAGORINSKY_KH           /*    Use Smagorinsky's nonlinear eddy */
                                /*  viscosity if SMAGORINSKY_KH is     */
                                /*  defined.  KH is the background.    */
#define SMAG_LAP_CONST 0.15     /* @  The nondimensional Laplacian     */
                                /*  Smagorinsky constant.  Often 0.15. */
#undef SMAGORINSKY_AH           /*    Use a biharmonic form of Smag-   */
                                /*  orinsky's nonlinear eddy viscosity */
                                /*  if SMAGORINSKY_AH is defined.      */
#define SMAG_BI_CONST 0.032     /* @  The nondimensional biharmonic    */
                                /*  Smagorinsky constant.  Often 0.015.*/
#define NOSLIP                  /*    This should be '#define NOSLIP'  */
                                /*  for no slip boundary conditions    */
                                /*  or '#undef NOSLIP' for free slip   */
                                /*  boundary conditions (the default). */
                                /*    The implementation of the free   */
                                /*  slip boundary conditions on a C-   */
                                /*  grid is much cleaner than the      */
                                /*  no slip boundary conditions.  The  */
                                /*  use of free slip b.c.s is strongly */
                                /*  encouraged.  The no slip b.c.s are */
                                /*  not implemented with the biharmonic*/
                                /*  viscosity.                         */

/*  Specify the horizontal interface depth diffusion.                 */
#undef  THICKNESSDIFFUSE        /*    If THICKNESSDIFFUSE is defined,  */
                                /*  interfaces are diffused with a     */
                                /*  coefficient of KHTH.               */
#define KHTH 500.0              /* @  KHTH is the interface depth      */
                                /*  diffusivity, in m2 s-1.            */

/*  Specify the properties of the passive tracers.                    */
#define MAXTR 3                 /*    The maximum number tracers (such */
                                /*  as T and S) that might be used.    */
#define KHTR 0.0                /* @  KHTR is the along-isopycnal      */
                                /*  tracer diffusivity, in m2 s-1. No  */
                                /*  KHTR is needed for numerical       */
                                /*  stability.  If this diffusion is   */
                                /*  not needed, memory is saved if KHTR*/
                                /*  is undefined.                      */

/*  Specify the scheme for the continuity equation.                   */
#define IORD 3                  /* @  If Smolarkiewicz's MPDATA is     */
```

```
                                /*  used to step the continuity        */
                                /*  equation, IORD is the number of    */
                                /*  iterations. IORD=1 is the donor    */
                                /*  cell scheme.  Results improve up to*/
                                /*  IORD ~ 4. IORD 2 or 3 are typical. */

#define P_REF 2.0e7             /*    P_REF is the pressure that is    */
                                /*  used for calculating the coordinate*/
                                /*  density, in Pa (=1e4 dbar).        */
#define RHO_0 1035.0            /*    RHO_0 is used in the Boussinesq  */
                                /*  approximation to calculations of   */
                                /*  pressure and pressure gradients,   */
                                /*  in units of kg m-3.                */
#define C_P 3925.0              /*    C_P is the heat capacity of sea  */
                                /*  water in J kg-1 K-1, approximated  */
                                /*  as a constant.                     */
#define G_EARTH 9.80            /*    G_EARTH is the Earth's gravi-    */
                                /*  tational acceleration, in m s-2.   */
```

Appendix B

Flow velocity with wind stress $\tau = 0.1$ N m^{-2}.

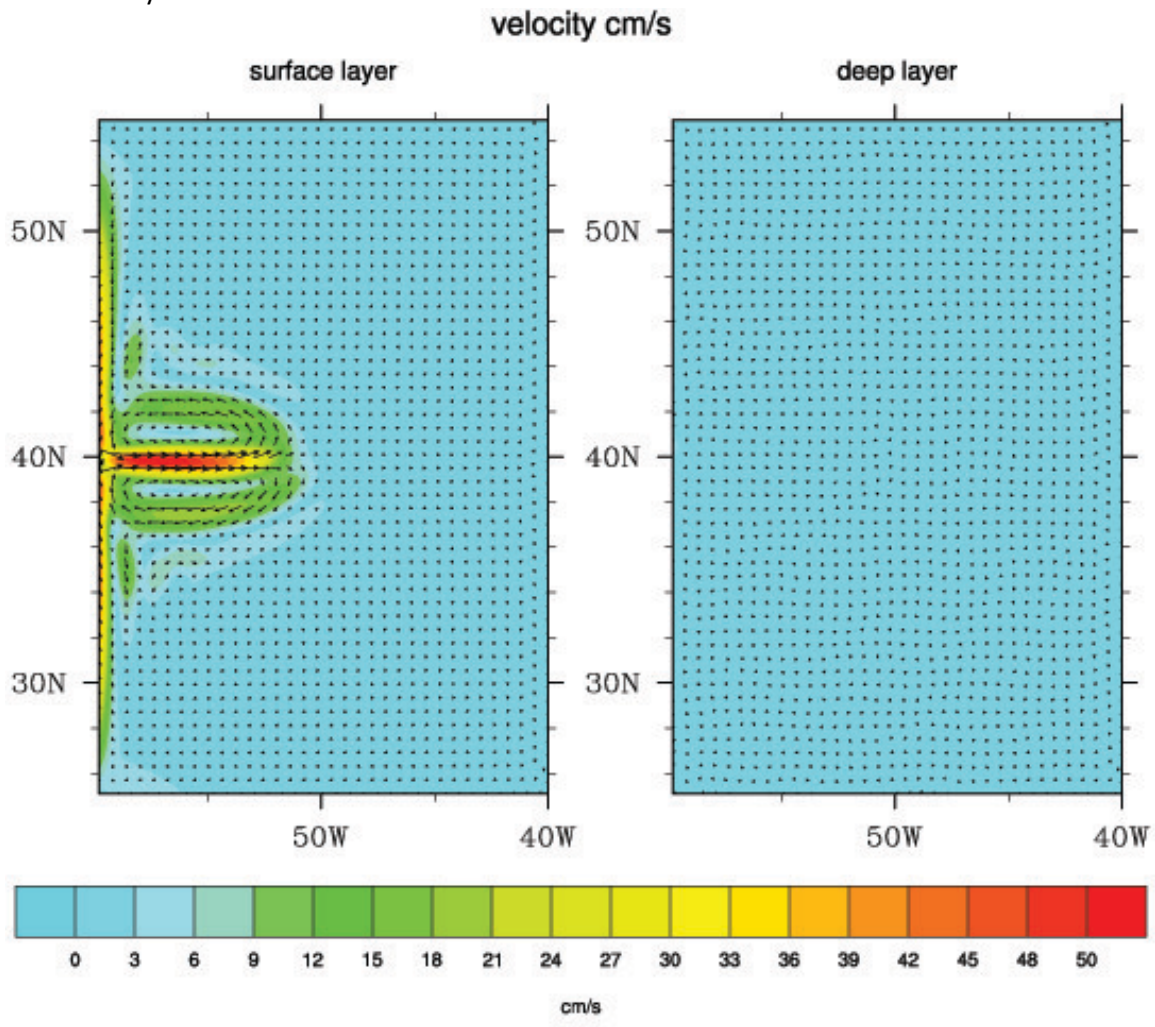

Flow velocity with wind stress $\tau = 0.2$ N m^{-2}.

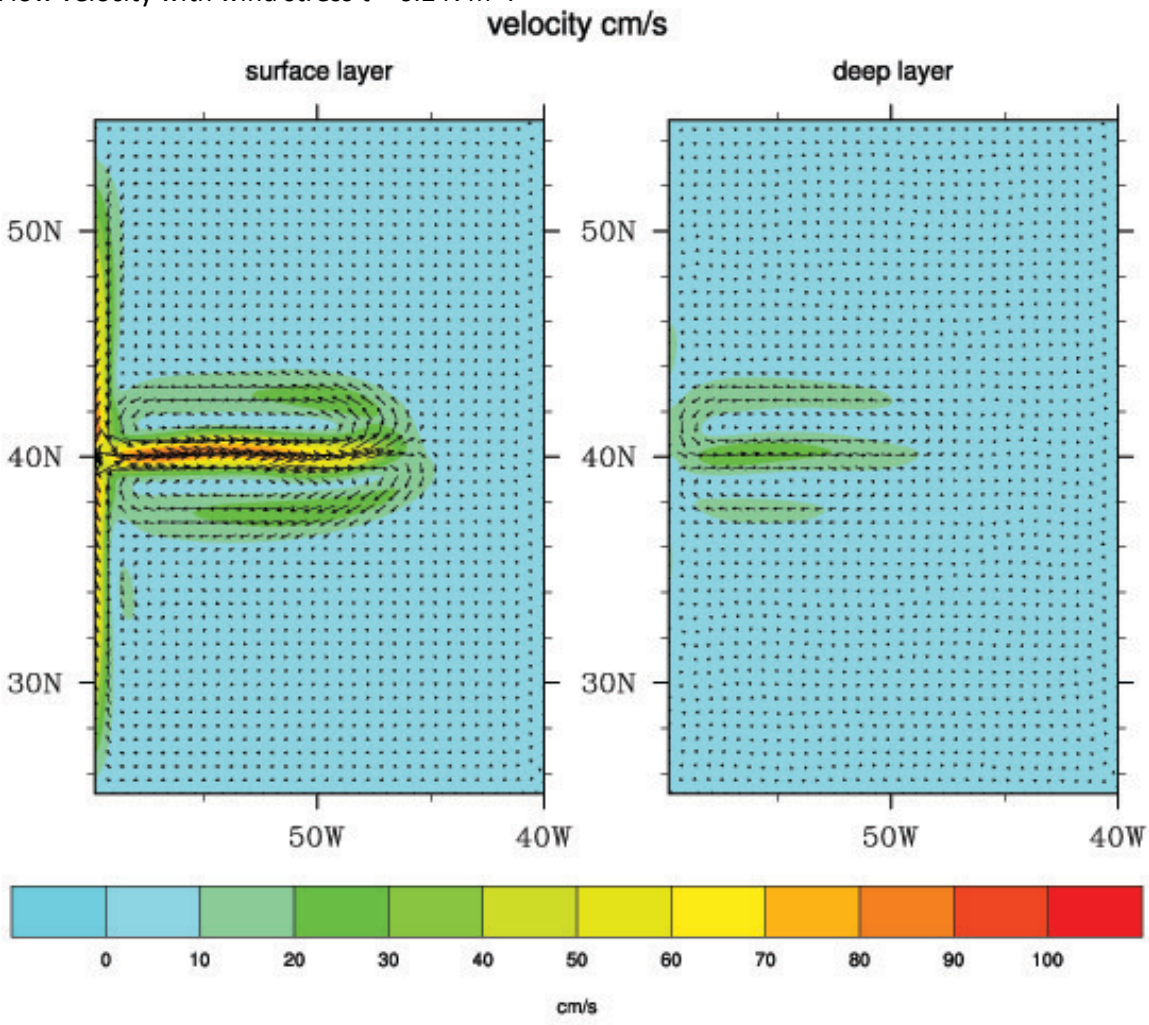

Appendix C

Tracer concentration snapshots:

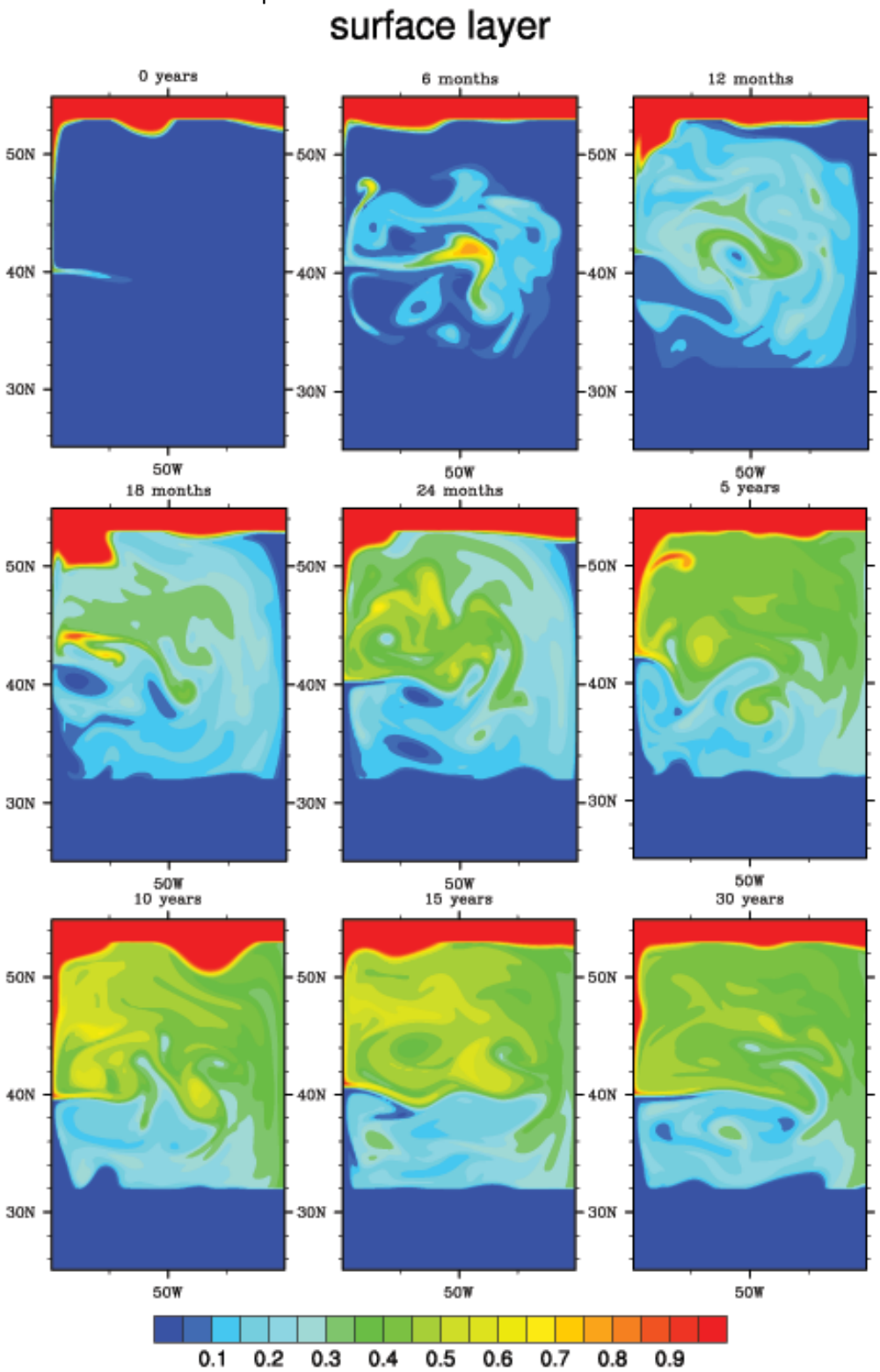

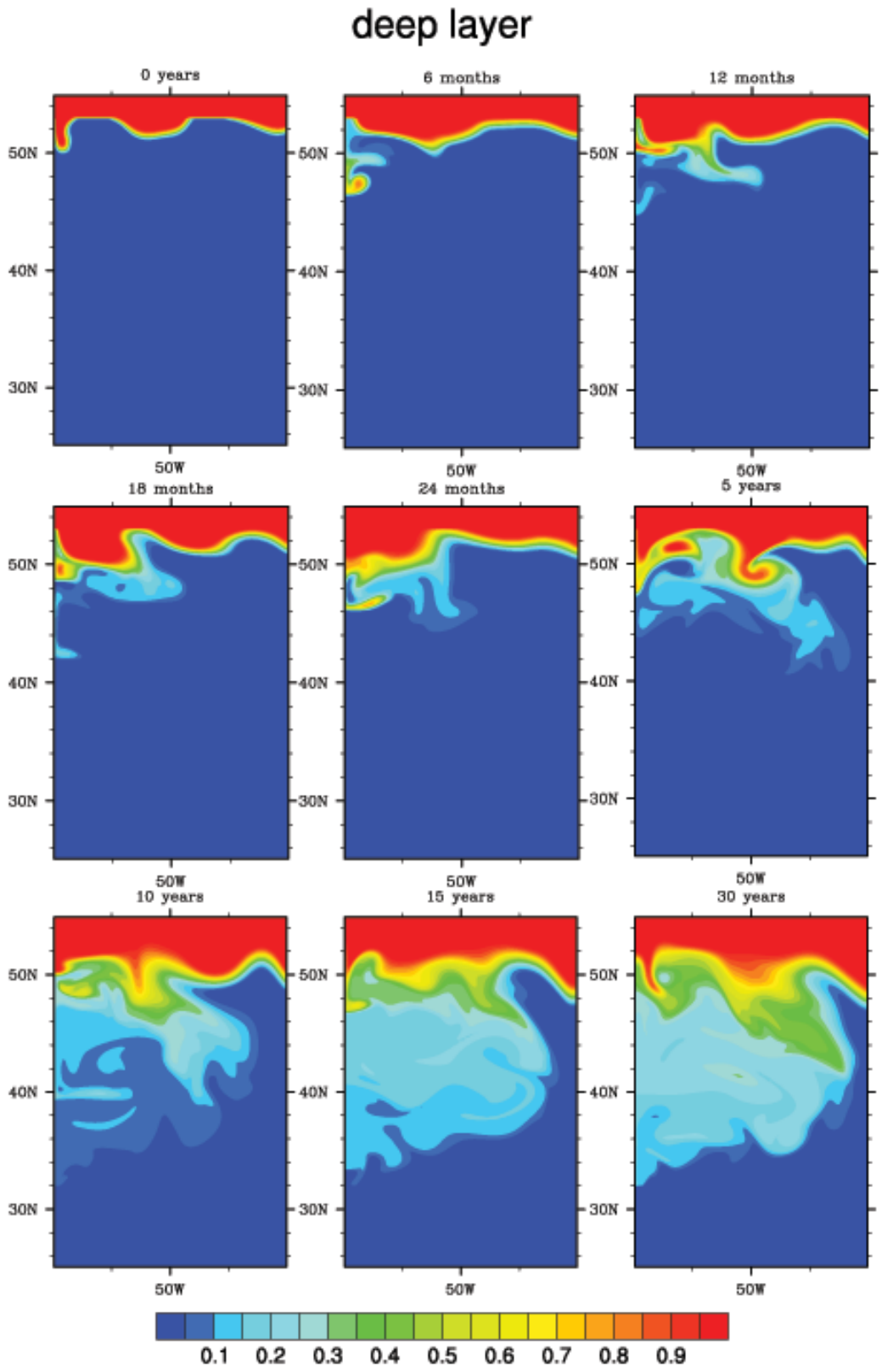
deep layer
0 years
6 months
12 months
18 months
24 months
5 years
10 years
15 years
30 years
50N
40N
30N
50W
0.1
0.2
0.3
0.4
0.5
0.6
0.7
0.8
0.9

Appendix D

Wind forcing 4 gyre system:

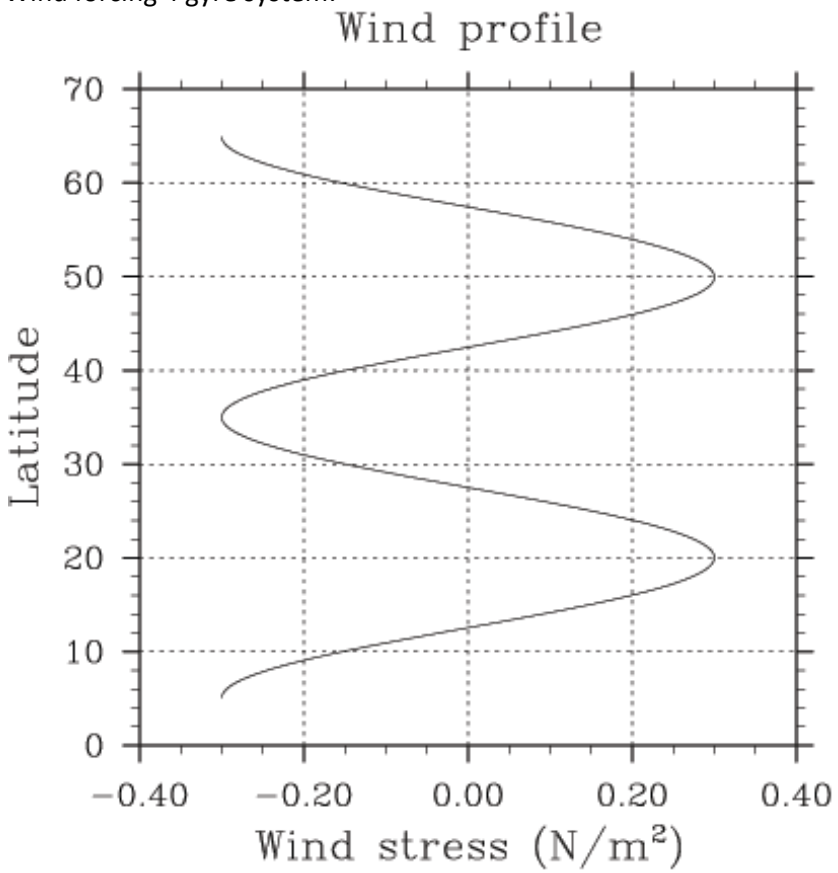

Appendix E

Tracer concentration snapshots 4 gyre system:

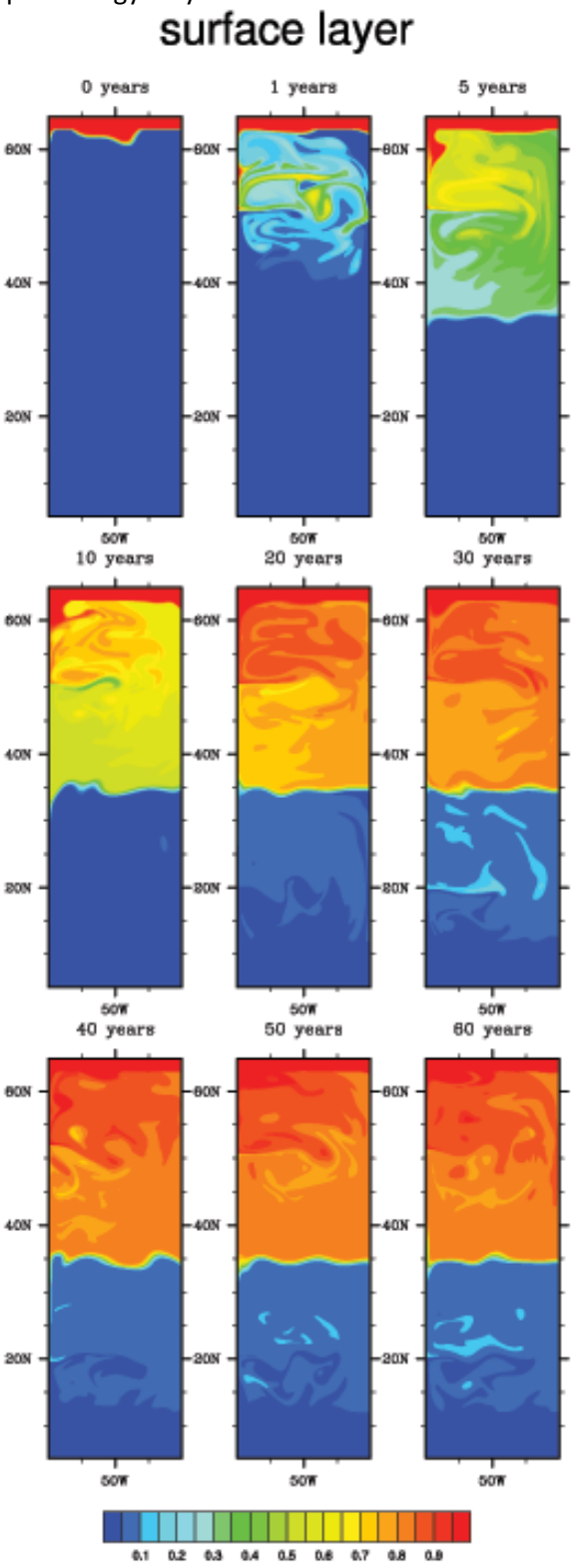

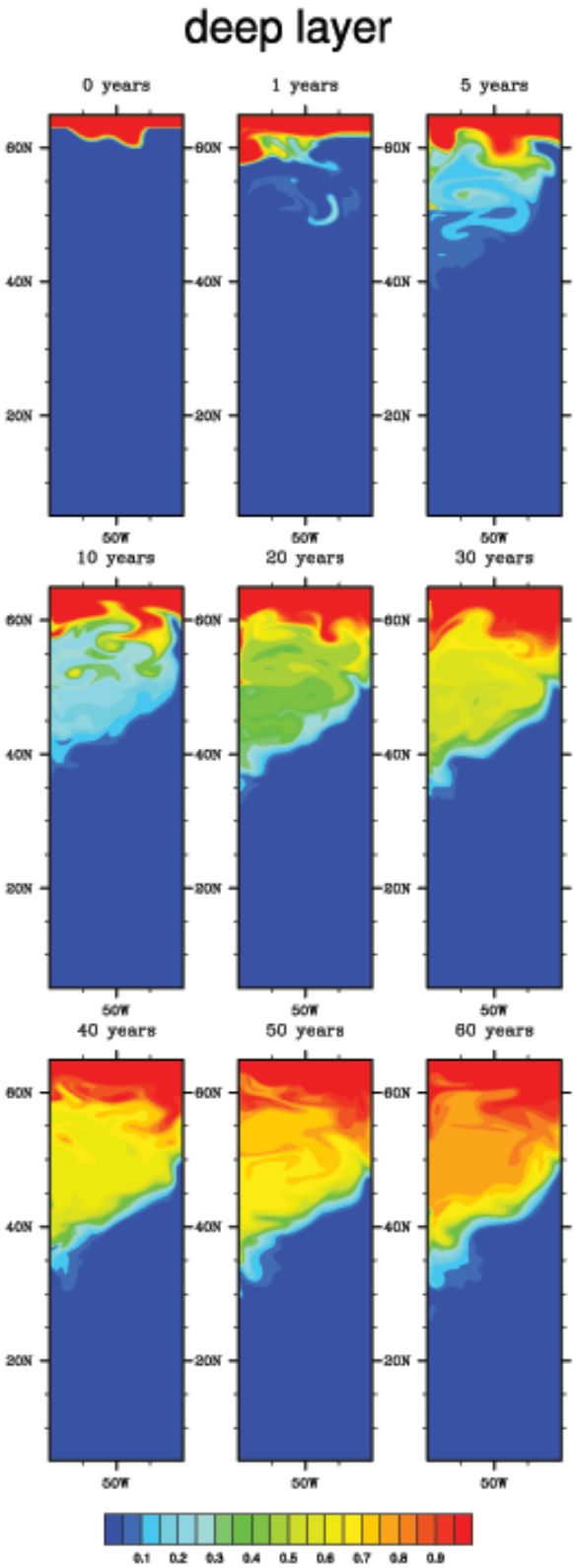
deep layer
0 years
1 years
5 years
10 years
20 years
30 years
40 years
50 years
80 years
60N
40N
20N
50W
0.1
0.2
0.3
0.4
0.5
0.6
0.7
0.8
0.9

Appendix F

Domain of schematised Atlantic Ocean with continental land boundaries:

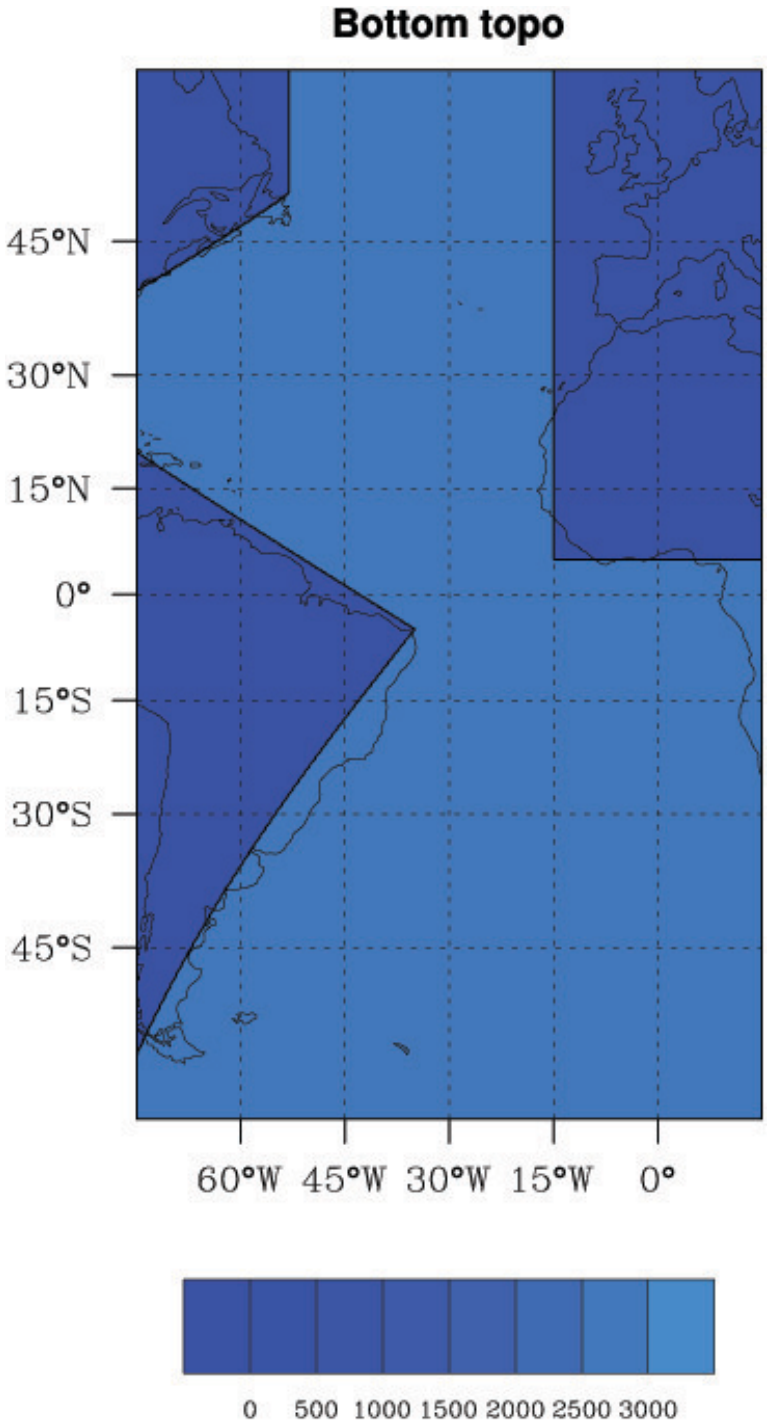

Wind stress on Atlantic Ocean with continental land boundaries:

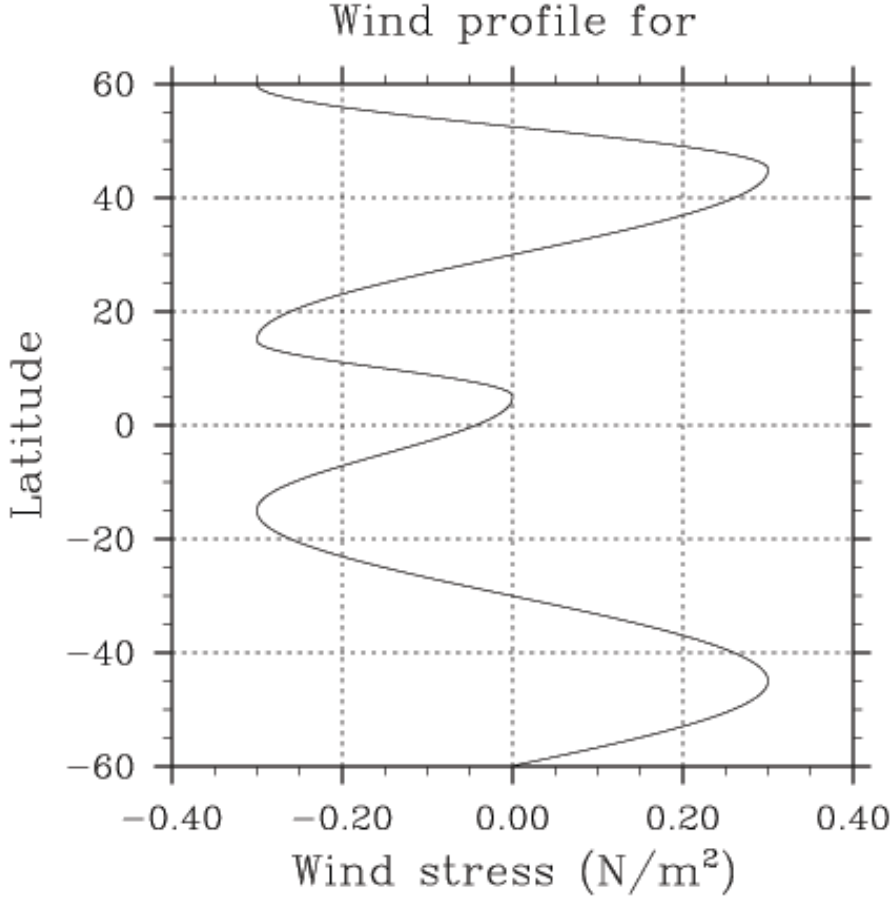

Appendix G

Eddy kinetic energy for schematised Atlantic Ocean with continental land boundaries: